Distances and charges along the Orai1 nexus-TM3 interface control STIM1-binding and pore opening

Julia Söllner[1], Magdalena Prantl[1], Hadil Najjar[1], Veronika Aichner[1], Ana Marija Suta[1], Yuliia Nazarenko[1], Selina Haranth[1], Maximilian Fröhlich[1], Diana Thallinger[1], Tamara Radiskovic[1], Christopher Mairhofer[3], William Nzegge[3], Sarah Weiß[1], Heinrich Krobath[2], Mario Waser[3], Isabella Derler[1,*]

[1] Institute of Biophysics, JKU Life Science Center, Johannes Kepler University Linz, Gruberstraße 40, 4020 Linz, Austria

[2] Institute of Theoretical Physics, Johannes Kepler University Linz, Altenbergerstraße 69, 4040 Linz, Austria

[3] Institute of Organic Chemistry, Johannes Kepler University Linz, Altenbergerstraße 69, 4040 Linz, Austria

[*] Corresponding author: Isabella.derler@jku.at, Phone +43732-2468-7612.

Abstract

Calcium (Ca^{2+}) influx through the Ca^{2+} release-activated Ca^{2+} (CRAC) channel is triggered by binding of the Ca^{2+} sensor Stromal Interaction Molecule 1 (STIM1) to the pore-forming Orai1 complex, primarily to its cytosolic C-termini. These C-termini connect to the transmembrane domain (TM) 4 via the flexible nexus region, proposed to transmit the activation signal from the STIM1-binding site to the central pore via concentrically arranged TM domains. However, the conformational dynamics of the nexus-TM3 interface required for channel gating remain elusive. Here, we investigate its role using unnatural amino acid (UAA)-based photo- and chemical crosslinking at individual positions within the nexus-TM3 interface combined with conventional site-directed mutagenesis. We report that a widening of the nexus-TM3 interface is essential for STIM1-mediated pore opening, while hydrophobicity and contact distances in the upper nexus-TM3 interface fine-tune signal propagation to the pore. These findings underscore the relevance of the nexus-TM3 dynamics for proper Orai1 function.

Introduction

Calcium ions (Ca^{2+}) are vital second messengers in numerous signaling pathways that regulate key cellular processes such as gene expression, muscle contraction, immune response, and cell proliferation [1–3]. One of the most prominent Ca^{2+} entry routes is the Ca^{2+} release-activated Ca^{2+} (CRAC) channel, which plays a crucial role especially in immune cells. It consists of the pore-forming protein Orai1 in the plasma membrane (PM) and the Ca^{2+} sensor Stromal Interaction Molecule 1 (STIM1) in the membrane of the endoplasmic reticulum (ER), the main Ca^{2+} store of a cell [4–7]. Upon ER Ca^{2+} store-depletion, STIM1 undergoes a conformational rearrangement, oligomerizes, and translocates to ER–PM junctions where it binds to and activates Orai1, thereby triggering Ca^{2+} influx [8–10]. Several mutations in either STIM1 or Orai1 can lead to loss- or gain-of-function (L-/GoF) of the CRAC channel complex. This can cause diseases such as severe immunodeficiencies, Stormorken-like syndrome or tubular aggregate myopathy, highlighting the physiological relevance and the need for a deeper understanding of the molecular mechanisms of the tightly controlled CRAC channel activation [11–13].

In this work, we focus on the human Orai1 (hOrai1) isoform denoted as Orai1. It forms a unique hexameric complex, whereof each monomer comprises four transmembrane (TM) helices, two extracellular and one intracellular loop, and a cytosolic N- and C-terminus. The six TM1 helices form the highly Ca^{2+} selective pore, which is enclosed by a ring of the six TM2-TM3 helices and TM4 in the periphery [14–17]. Pore opening is initiated by STIM1-binding to its main coupling site, the C-terminus of Orai1, triggering a series of conformational changes across the entire channel, resulting in pore opening [12,18–22]. The Orai1 C-terminus is connected via the so-called nexus region to TM4, which has been reported to be important for pore opening [23]. The flexible nexus region consists of two segments – the lower flexible nexus (K265, H264, S263) and the upper hydrophobic nexus (V262, L261) (Fig. 1a). It is highly conserved in *Drosophila melanogaster* Orai (dOrai) and a structural comparison between the closed and open dOrai crystal structures suggests that the kinked, antiparallel C-termini in the resting conformation unlatch and straighten upon channel activation (Fig. 1a) [14,16]. While such conformational changes appear less pronounced in the corresponding cryo-EM structures (PDB: 7KR5)[15], cysteine cross-linking studies on the Orai1 C-terminus again indicate its conformational change upon STIM1-coupling [24]. A recent study by Zhou et al.[23] proposes that STIM1-binding provokes a bending of the lower flexible nexus, which propagates to the upper nexus-TM3 interface to induce pore opening. We recently published that non-pore-lining TM interfaces, which are connected to the nexus region at the cytosolic side, undergo STIM1-induced widening crucial for pore opening [25]. However, the exact conformational changes and the role of the nexus-TM3 interface in the physiologically relevant STIM1-mediated pore opening process still remain unclear.

To uncover the molecular mechanism and essential conformational rearrangements within the Orai1 channel complex, we successfully demonstrated that the emerging genetic code expansion (GCE) technology is a powerful tool [25,26]. Thereby, an orthogonal aminoacyl-tRNA synthetase/tRNA pair is introduced into the host organism, enabling the incorporation of a certain unnatural amino acid (UAA) at a site-specifically introduced amber stop codon (TAG) during the native ribosomal translation [27,28].

In this study, we used this technique to introduce UAAs with photo- and chemical crosslinking capabilities into the Orai1 nexus-TM3 interface to gain, combined with functional studies, a deeper and more precise understanding of conformational dynamics within this region during channel opening. We seek to uncover another missing piece of the puzzle in understanding the molecular mechanisms by which the STIM1-activation signal is transmitted from the peripheral C-terminus, through the nexus, to the entire channel complex and the central pore of Orai1.

Results

Photocrosslinking UAAs at sites in the nexus and opposite in TM3 allow upon STIM1-mediated activation UV-induced current reduction

To shed light on the exact conformational dynamics within the nexus and its interactions with TM3 critical for STIM1-mediated activation, we incorporated photocrosslinking UAAs, specifically p-azido-L-phenylalanine (Azi) and p-benzoyl-L-phenylalanine (Bpa) (Fig. 1b), both capable of forming a covalent bond with any residue within 3-4 Å upon UV-light exposure[29,30], within this region.

An initial mutational screen with photocrosslinking UAAs, Azi or Bpa, through the nexus region (^{261}LVSHK^{265}) revealed one outstanding site, K265. Insertion of Azi at this position (Orai1 K265Azi) leads to significantly increased Orai1 wild-type (WT) currents upon STIM1 co-expression before exposure to UV-light, which were significantly reduced upon UV-illumination to current levels under WT conditions (Fig. 1c,d). In a negative control experiment, the Orai1 C-terminal mutation L273D, that impairs STIM1-binding and STIM1-mediated activation[31], also blocked STIM1-induced activation of Orai1 K265Azi L273D (Supp. Fig. 1a). The current/voltage (I/V) relationship of STIM1 + Orai1 K265Azi currents showed a comparable robust inward rectification and a reversal potential of approximately +50 mV like STIM1-mediated Orai1 WT currents (Fig. 1e). Fast Ca^{2+} dependent inactivation (FCDI) was reduced compared to that of STIM1-mediated Orai1 WT currents and was followed by a reactivation phase (Fig. 1f), which might be related to the strongly increased store-operated currents. To investigate whether the elevated store-operated currents of Orai1 K265Azi or the reduction in current size after UV-light exposure were due to changes in interactions with STIM1, fluorescence resonance energy

103 transfer (FRET) of Orai1-YFP K265Azi with STIM1-CFP compared to WT conditions was
104 measured before and after store-depletion via Thapsigargin (TG) and following UV-exposure.
105 No significant changes in the FRET efficiency were detected using these different conditions
106 (Fig. 1g, Supp. Fig. 1b), which indicates comparable STIM1-binding to Orai1 WT and Orai1
107 K265Azi.

108 In contrast to Orai1 K265Azi, Azi substitutions of other residues along the nexus led to smaller
109 STIM1-mediated currents compared to Orai1 WT. Orai1 H264Azi showed a significant UV-
110 mediated current reduction following maximal STIM1-induced activation and for Orai1
111 S263Azi, a similar tendency was observed (Fig. 1c). Among the corresponding Bpa-nexus mu-
112 tants, also Orai1 K265Bpa tended to exhibit enhanced currents compared to Orai1 WT, which
113 reduced slightly after UV-exposure, whereas other Bpa-nexus mutants showed only weak
114 STIM1-mediated activation, which did not alter after UV-illumination (Supp. Fig. 1c).

115 As several side chains in TM3 point directly towards the nexus region (Fig. 1h), we performed
116 a second screen by incorporating Azi/ Bpa at positions in TM3 which are located opposite to
117 the nexus. Here, Orai1 R167Azi showed significantly enhanced STIM1-mediated currents with
118 UV-induced current reduction to WT-like levels (Fig. 1i,j). The I/V relationship was like WT (Fig.
119 1k), whereas FCDI occurring within 50ms, was less pronounced compared to Orai1 WT and
120 was followed by a reactivation phase (Fig. 1l). The binding of Orai1-YFP R167Azi and STIM1-
121 CFP appears unaltered as indicated by FRET experiments (Fig. 1m, Supp. Fig. 1b). Upon Bpa
122 incorporation, a similar, but not significant trend was detected for Orai1 R167Bpa (Supp. Fig.
123 1d).

124 Towards the upper nexus, the incorporation of Azi but not Bpa at Orai1 H171 resulted in WT-
125 like currents, that were drastically increased upon UV-illumination (Fig. 1i, Supp. Fig. 1d). A
126 similar UV-induced current enhancement yet upon introducing Bpa rather than Azi was ob-
127 served for Orai1 L174Bpa, as published in our previous study[26] (Fig. 1i, Supp. Fig. 1d). Other
128 corresponding Azi- or Bpa-mutants along the upper nexus exhibited STIM1-mediated activa-
129 tion similar to Orai1 WT and were unaffected by UV-light exposure.

130 Our UAA-containing mutants showed neither constitutive activity nor UV-induced current alter-
131 ations in the absence of STIM1 as shown for all Azi-mutants and selected Bpa-mutants (Supp.
132 Fig. 1e,f). Only Orai1 L174Bpa exhibits UV-induced activation already in the absence of STIM1
133 (Fig. 1f), as already discovered in our previous study [26].

134 Summarizing, UV-exposure upon UAA-incorporation in and opposite to the lower nexus region
135 (K265, R167) results in strong STIM1-mediated currents and UV-induced current reduction. In
136 contrast, UV-illumination of UAAs in TM3 facing the upper nexus region (H171, L174) leads to
137 robust STIM1-mediated current increases.

138 **Aromatic substitutions at K265 increase STIM1-mediated currents of Orai1**

139 Since for both positions, K265 and R167 (Fig. 2a), in particular the incorporation of the bulky
140 Azi, resulted in significantly enhanced STIM1-mediated currents, we hypothesized that a wid-
141 ening of the nexus-TM3 interface due to the increased size of the inserted UAA, could be
142 responsible for the enhanced current size. We further speculate that the UV-mediated current
143 reduction is potentially associated with a nexus-TM3 distance dependence. To probe for a re-
144 lation between distance and current size, we mutated K265 and R167 to bulky aromatic as
145 well as small amino acids for negative control (K265A/F/Y/W; R167A/F/Y/W). Indeed, electro-
146 physiological experiments revealed significantly enhanced STIM1-mediated currents for Orai1
147 K265F/Y compared to Orai1 WT but not for Orai1 K265A (Fig. 2b,c). Despite the greatly in-
148 creased currents, the I/V-relationship of STIM1-mediated currents was similar to Orai1 WT, as
149 exemplarily shown for Orai1 K265Y (Fig. 2d). Orai1 K265W, similar to Orai1 K265Bpa, showed
150 a tendency for, but not significantly increased currents compared to WT conditions (Fig. 2c),
151 probably due to steric interference of the bulky tryptophan or the formation of inhibitory hydro-
152 phobic interactions.

153 In contrast, maximum WT-like STIM1-mediated currents were observed for Orai1 R167 mu-
154 tants, regardless of the size of the incorporated amino acid (Fig. 2e). Next, we introduced
155 double point mutations (R167A/F/Y/W K265A/F/Y/W) to test whether the current could be en-
156 hanced. Only for the mutants, Orai1 R167Y K265Y and Orai1 R167W K265Y, STIM1-mediated
157 currents were significantly increased compared to WT, albeit not reaching the level of the Orai1
158 K265Y single mutant (Fig. 2f,g). The FRET signal was significantly lower for Orai1 R167Y
159 K265Y, but not for Orai1 K265Y compared to Orai1 WT, indicating altered STIM1-binding for
160 the double-Y mutant (Fig. 2h). Interestingly, the current size of Orai1 R167F K265F was mark-
161 edly lower than that of the single mutant Orai1 K265F (Fig. 2c,g), possibly due to local for-
162 mation of inhibitory hydrophobic interactions, which might reflect in reduced backbone flexibility
163 and the suppression of the propagation of the opening signal.

164 In summary, increasing the amino acid side chain size at position K265 but not at position
165 R167, both situated in the nexus-TM3 interface, increases STIM1-mediated currents. Some
166 double aromatic substitutions at these positions can enhance currents but also impair STIM1-
167 coupling compared to Orai1 WT.

168 **Alanine substitutions in TM3 opposite the UAA in the nexus leave UV-mediated current**
169 **decrease unaffected, but, in some cases, decrease STIM1-induced maximal activation**

170 Since bulky aromatic side chains along the nexus trigger significant enhancements of STIM1-
171 mediated currents, we hypothesized that the observed decrease in STIM1-induced currents
172 after UV-light application could be due to a decrease in the distance of the nexus region caused

173 by photocrosslinking. We therefore tested whether a reduction in side-chain sizes of residues
174 at critical positions in TM3 opposite to a UAA in the nexus region could counteract UV-induced
175 current reduction. Hence, we combined Orai1 K265Azi with mutations in TM3 (E166, R167,
176 R170) to alanine (Fig. 3a). However, for all double or triple mutants, UV-illumination still re-
177 sulted in current decrease after maximal STIM1-induced activation before UV-light exposure
178 (Fig. 3b, Supp. Fig. 2a). Interestingly, the combination of K265Azi with E166A or in some cases
179 R170A revealed approximately 50% lower STIM1-mediated maximal currents compared to
180 Orai1 K265Azi alone. Notably, double or triple mutants showing similar maximal currents like
181 Orai1 K265Azi exhibited UV-induced current reduction to levels 50% reduced compared to WT
182 conditions. In contrast, mutants exhibiting reduced maximal STIM1-mediated currents com-
183 pared to Orai1 K265Azi, revealed UV-mediated current decrease even 75% reduced compared
184 to those under WT conditions. Overall, this might be related to the reduced side chain volume.
185 FRET levels were also significantly reduced for Orai1-YFP K265Azi E166A and Orai1-YFP
186 K265Azi E166A R167A/R170A compared to Orai1 K265Azi and Orai1 WT, all co-expressed
187 with STIM1-CFP (Fig. 3c). Hence, STIM1-binding to these double and triple mutants might be
188 affected, potentially acting as another cause for decreased current levels. Thus, reducing
189 amino acid side chain size of oppositely located residues does not eliminate UV-induced de-
190 activation, but in some cases can lead to overall lower current density levels than for STIM1-
191 activated Orai1.

192 A similar approach was performed for Orai1 R167Azi, in which different residues close to or
193 opposite R167 (E166, R170, H264, K265) were mutated again to an alanine (Fig. 3a). Analo-
194 gous to mutant Orai1 K265Azi, all tested Orai1 R167Azi-alanine-mutants showed STIM1-me-
195 diated activation, which reduced after UV-exposure (Supp. Fig. 2b). Interestingly, the combi-
196 nation of R167Azi with E166A or with H264A resulted in lower STIM1-mediated currents fol-
197 lowed by further UV-induced current reductions below levels reached under WT conditions
198 (Fig. 3d). While FRET levels for the double mutant Orai1 R167Azi E166A were similar to
199 R167Azi under resting conditions as well as after store-depletion (Fig. 3e). This highlights
200 again a potential role of side chain size at the nexus-TM3 interface in STIM1-induced Orai1
201 activation.

202 In conclusion, decreasing side chain size in the surroundings of Orai1 K265Azi or Orai1
203 R167Azi is not sufficient to eliminate the UV-induced reduction of STIM1-mediated currents.
204 Nevertheless, in combination with E166A and R170A or H264A, respectively, both K265Azi
205 and R167Azi showed strongly decreased STIM1-mediated current levels, indicating an im-
206 portant function of their local interaction partners in the nexus-TM3 interface in pore opening
207 and/or signal transduction.

208 **Combination of K265Azi/Bpa or R167Azi/Bpa with mutations triggering constitutive ac-**
209 **tivity eliminates UV-induced current decrease**

210 Next, we investigated the effect of combining K265Azi or R167Azi with mutations within Orai1
211 which alone led to constitutive Ca^{2+} influx also under store-replete conditions. Here, we focused
212 on several known GoF-mutations located across all four TM domains including V102A in TM1,
213 H134A in TM2, V181K in TM3 and V181W A254W in TM3-TM4 (Fig. 4a). All of them lead to
214 constitutively active Orai1 currents with almost CRAC channel-like I/V relationship and reversal
215 potential[32,33] (Fröhlich et al., unpublished), except V102A resulting in non-selective constitutive
216 currents [34]. While V102A disrupts the hydrophobic gate in the pore[35], H134A destabilizes the
217 closed state by abolishing the function of the histidine as a steric brake [36]. For V181K[37] and
218 V181W A254W (Fröhlich et al., unpublished), we reported that they affect the non-pore-lining
219 TM interfaces, involving their widening, which in turn contributes to constitutive pore opening.
220 Hence, it is known that V181K and V181W A254W affect the TM3-TM4 interface, while it re-
221 mains unclear whether V102A and H134A also impact the peripheral channel segments.
222 Therefore, we speculated that photocrosslinking of K265Azi impacts Orai1 V102A and Orai1
223 H134A differently than Orai1 V181K and Orai1 V181W A254W. The combination of the different
224 GoF-mutations with K265Azi led in all cases to constitutive currents in the absence of STIM1
225 co-expression (Fig. 4b,c) with I/V relationships and reversal potentials comparable to previous
226 reports, as exemplarily shown for Orai1 K265Azi V102A/H134A/V181K (Supp. Fig. 3a) [32,37,38].
227 However, these mutation combinations eliminated the UV-induced current decrease (Fig.
228 4b,c). This indicates that the GoF-mutations trigger different conformational changes in the
229 nexus-TM3 interface than STIM1, which hinder functional effects of UV-illumination. In the
230 presence of STIM1, all double mutants exhibited constitutively active currents with I/V-relation-
231 ships reaching a reversal potential of around +50 mV for Orai1 K265Azi V102A/H134A/V181K
232 (Supp. Fig. 3b), consistent with previous studies [32,37,38]. Interestingly, in the presence of STIM1,
233 UV-induced photocrosslinking had a slight, but no significant effect on the tested Orai1 GoF-
234 K265Azi mutants (Fig. 4d,e). STIM1-binding was not negatively affected as exemplarily shown
235 for STIM1-CFP and Orai1 K265Azi V181K-YFP (Supp. Fig. 3c). Also, for Orai1 R167Azi V181K
236 only a weak UV-induced current reduction was observed in the absence as well as in the pres-
237 ence of STIM1 (Fig. 4f).

238 Additionally tested Bpa-mutants (Orai1 K265Bpa V181K, Orai1 R167Bpa V181K) again exhib-
239 ited no significant UV-mediated current decrease in the absence or presence of co-expressed
240 STIM1 (Supp. Fig. 3d).

241 Furthermore, we investigated the nexus mutant Orai1 H264Azi in combination with GoF-mu-
242 tants H134A and V181K. For both GoF-H264Azi mutants, constitutive activity but no significant

243 effect of UV-light illumination on current size was observed, both in the absence and presence
244 of STIM1 (Supp. Fig. 3e).

245 These results indicate that UV-induced photocrosslinking of K265Azi, H264Azi or R167Azi in
246 the presence of the tested GoF-mutations is unable to induce conformational changes along
247 the nexus-TM3 interface in the absence of STIM1. We hypothesize that, due to a structural
248 change in this peripheral channel segment, such as putative widening of the non-pore-lining
249 TM interface in the GoF-mutants, Azi at K265 and R167 can hardly reach its crosslinking part-
250 ner. STIM1 seems to induce some structural changes at the nexus-TM3 interface which allow
251 at least for the TM3-TM4 GoF-mutants slight, but not significant UV-induced functional changes
252 due to potential structural rearrangements in this peripheral channel segment.

253 Taken together, UV-induced current decrease of Orai1 K265Azi, Orai1 H264Azi and Orai1
254 R167Azi is lost in combination with all tested GoF-mutations even in the presence of STIM1.

255 **Restraining the nexus-TM3 interface via photo- and chemical crosslinking impairs**
256 **STIM1-mediated maximal activation**

257 As we assume a widening along the nexus-TM3 interface during STIM1-binding and channel
258 opening, we wondered whether exposure to UV-light prior to STIM1-binding might interfere
259 with opening-relevant conformational changes to occur and thereby lower maximal current
260 size. To this end, we compared the effects of two different experimental activation protocols on
261 critical Orai1 UAA-mutants in the patch-clamp experiment: i) the initial application of UV-light
262 immediately after entering the whole-cell configuration, hence, before STIM1 binds to the Orai1
263 mutant, followed by passive store-depletion-induced STIM1-mediated activation and ii) allow-
264 ing for STIM1-binding and maximal STIM1-mediated currents to be reached and subsequent
265 illumination of UV-light for photocrosslinking, as in previously shown measurements. Indeed,
266 UV-exposure before STIM1-binding nearly abolished STIM1-mediated currents for Orai1
267 K265Azi. Similar results were detected for some K265Azi-double and triple mutants, as exem-
268 plarily shown for Orai1 K265Azi E166A and Orai1 K265Azi E166A R167A (Fig. 5a,b). Hence,
269 the UV-induced photocrosslink of K265Azi hinders STIM1-mediated activation of the channel,
270 probably by preventing conformational rearrangements of the nexus-TM3 interface, that might
271 be necessary for proper pore opening. STIM1-binding itself is not impaired by applying UV-
272 light prior to STIM1-binding, as FRET measurements showed similar results to Orai1 WT for
273 both experimental conditions (Supp. Fig. 4a).

274 Also for Orai1 R167Azi, UV-illumination before STIM1-binding led to much lower currents than
275 STIM1-binding followed by UV-illumination, still reaching WT-like current levels (Fig. 5c).
276 FRET-levels for R167Azi were similar to Orai1 WT regardless of the UV-exposure (Supp. Fig.
277 4b).

278 Next, we used chemical crosslinking UAAs, namely a series of tyrosine analogues containing
279 the haloalkane bromine linked with aliphatic chains of varying length (BC_nY) (Fig. 5d). We de-
280 note our UAAs BetY, BprY and BptY for a modified tyrosine with added bromoethane, bromo-
281 propane and bromopentane, respectively. The chemical crosslinking UAA binds spontane-
282 ously, covalently and selectively via a nucleophilic reaction to the thiolate of a cysteine in close
283 proximity[29,39,40] and allows us to restrain the distance between two positions (e.g. E166C K265-
284 BC_nY). Whereas Orai1 K265-BetY alone showed WT-like current levels after STIM1-activation,
285 the STIM1-mediated current for the double mutant Orai1 K265-BetY E166C was significantly
286 reduced (Fig. 5e, Supp. Fig. 4c). Similar results were detected for the one CH-bond-longer
287 BprY. The double mutant Orai1 K265-BprY E166C exhibited strongly reduced currents
288 whereas the single mutant Orai1 K265-BprY reached current levels higher than WT. Addition-
289 ally, we examined the effect of BptY, three aliphatic repeat units longer than BetY, at K265 in
290 Orai1 E166C and discovered again lower current than when integrated in Orai1 WT (Fig. 5e).
291 Overall, all chemical crosslinking UAAs independent of side-chain length allow crosslinking
292 with opposite cysteine, while distinct store-operated current levels in the absence of E166C
293 might be assigned to distinct expression levels. Previous literature suggests that these chem-
294 ical crosslinking UAAs can reach their counterpart within the range of up to 15Å[41], which
295 matches with mean distance of backbone ($C\alpha$) to backbone of 12Å ± 0.37 and with interatomic
296 mean distance of 18Å ± 1.69 between the negatively charged carboxyl oxygen (COO^-) of E166
297 and the amino nitrogen (NH_3^+) of K265 estimated from our MD simulation on the Orai1 homol-
298 ogy model based on dOrai published in Najjar et al.[25] (Supp. Fig. 5a)

299 In contrast, the double mutant Orai1 K265-BetY R167C showed a current size comparable to
300 that of Orai1 K265-BetY alone (Supp. Fig. 4d). A reason could be that the chemical crosslinker
301 is too short to reach R167C and therefore the nexus-TM3 interface is still able to widen/rear-
302 range during STIM1-binding. Indeed, the longer BptY at K265 led to lower currents in combi-
303 nation with R167C compared to the Orai1 K265-BptY mutation alone.

304 To further prove that conformational rearrangements along the nexus-TM3 interface are es-
305 sential for STIM1-mediated pore opening, we performed cysteine-crosslinking experiments al-
306 lowing a reversible formation of a disulfide bond between two cysteines in close proximity via
307 the addition of diamide for cysteine crosslinking and BMS (Bis(2- mercaptoethyl)sulfone) for
308 reducing disulfide bonds back to the free sulfhydryl groups, respectively. For all four tested
309 mutants (two controls: Orai1 and Orai1 K265C and two test mutants: Orai1 K265C E166C and
310 Orai1 K265C R167C), STIM1-binding resulted in WT-like Ca^{2+} currents of the single and dou-
311 ble cysteine mutants. The subsequent addition of diamide decreased current levels signifi-
312 cantly for both Orai1 K265C E166C and Orai1 K265C R167C, likely due to formation of a
313 cysteine crosslink, whereas no current decrease was observed for both control conditions (Fig.

5f, Supp. Fig. 4e). The break of the disulfide bond via BMS restored initial current levels for K265C E166C and K265C R167C but did not drastically affect WT and K265C (Fig. 5f). Hence, we were able to reversibly modulate STIM1-mediated currents by reversible formation of a cysteine crosslink between K265 in the nexus and an opposite residue in TM3 (E166, R167).

Overall, these results showed that crosslinking within the nexus-TM3 interface can hinder proper STIM1-mediated pore opening, likely due to restricted STIM1-mediated conformational changes involving a widening.

STIM1-coupling to and STIM1-mediated activation of Orai1 require charges in the nexus-TM3 interface

Considering that Orai1 K265Azi E166A led to reduced STIM1-mediated coupling and activation, as well as that most residues in and opposite the nexus are charged, we pursued with analyzing the relevance of these charges in more detail (Fig. 6a). To back up our experimental protocol on charge substitutions as described below, we first investigated the apparent pKa values of the relevant residues E166, R167, H264 and K265 theoretically using both the PROPKA 3 package[42,43] as well as a Monte-Carlo based titration procedure based on the linearized Poisson-Boltzmann equation (MC-PBE)[44–47] on the homology model of hOrai1[48] based on the closed X-ray structure of dOrai (PDB: 4HKR)[14]. Orai1 E166, R167 and K265 showed monomer-independent results with apparent pKa values of 3.58, 12.94 and 10.07 in PROPKA, respectively (Supp. Fig. 6). The MC-PBE analysis revealed a clear pH independent preference of the respective charged side chains and the absence of a Henderson-Hasselbalch transition in these residues. Also, for H264, the results were monomer-independent in PROPKA, which predicted an apparent pKa of 7.14. However, in the MC-PBE approach the pKa of H264 was monomer-dependent and a strong tendency to retain the positive net charge in the imidazole ring at pH 7 with protonation probabilities ranging from 70% to 100% was reported (Supp. Fig. 6). This finding reflects considerable change with respect to the typical pKa value of 6.6 of histidine in folded proteins [49]. Hence, our theoretical analysis shows that all relevant residues in the nexus region have a distinct preference for engaging their charged states at pH 7 and motivates us to proceed with our following mutation strategy focusing on charge deletions and charge swaps to underscore the relevance of intra- and intermolecular salt bridges in the nexus region during STIM1-Orai1 association.

In a first step, we individually mutated charged residues in TM3 and the nexus to an alanine. Most alanine-mutants (K265, R167, R170, H171A) showed STIM1-mediated currents rather similar to Orai1 WT, except Orai1 E166A and Orai1 H264A (Fig. 6b, Supp. Fig. 7a), which exhibited significantly decreased STIM1-mediated currents. This indicates an important function in STIM1-mediated Orai1 activation of the negatively charged glutamic acid at position 166 and the positively charged histidine at position 264 (Supp. Fig. 6). Indeed, combination of

350 H264A with neutralizing mutations in the nexus and TM3 (H264A K265A, R167A H264A) which
351 alone retained current unaffected, reduced STIM1-mediated currents (Supp. Fig. 7b). Interest-
352 ingly, double and triple mutant combinations with E166A (E166A R167A, E166A R167A K265A,
353 E166A R167A H264A K265A) exhibited restored STIM1-mediated current levels like Orai1 WT.
354 Other combinations (R167A K265A, R170A H171A) showed comparable or slightly enhanced
355 STIM1-induced currents compared to WT (Supp. Fig. 7b). Nevertheless, FRET levels of Orai1-
356 YFP E166A/ R167A K265A and E166A R167A K265A in combination with STIM1-CFP showed
357 comparable results to STIM-CFP + Orai1 WT-YFP (Supp. Fig. 7c).

358 Next, we substituted a positively charged amino acid by a negatively charged one and vice
359 versa. Here, we were indeed able to show reduced current size for Orai1 E166R as well as for
360 Orai1 K265E, but not for Orai1 R167E and R170E (Fig. 6c; Supp. Fig. 7d). FRET-levels for
361 these mutants were similar to WT, suggesting unaltered STIM1-Orai1 binding (Fig. 6d).

362 Finally, we combined charge replacement mutations in the nexus and opposite in TM3. We
363 observed significantly lower STIM1-mediated currents for Orai1 R167E K265E and Orai1
364 R170E K265E than for WT (Fig. 6e). Even in FRET-experiments, the maximal FRET-levels
365 after TG treatment were significantly reduced for the double mutants Orai1 R167E K265E and
366 Orai1 R170E K265E (Fig. 6f). For another mutant, Orai1 E166R H264R, STIM1-mediated cur-
367 rents were even abolished (Fig. 6e).

368 In summary, charged residues at the nexus-TM3 interface are crucial for STIM1-binding and
369 pore opening, as charged substitutions at certain positions led to decreased Orai1-STIM1-
370 binding efficiency as well as low STIM1-mediated currents.

371 **Photocrosslinking UAAs located on the opposite side of the upper hydrophobic nexus**
372 **exhibit strong UV-mediated current activation**

373 In contrast to all UAA-containing mutants in the lower nexus-TM3 interface showing UV-medi-
374 ated reduction of STIM1-triggered maximal currents, two mutations in the upper nexus-TM3
375 interface, namely H171Azi and L174Bpa depicted a strong UV-mediated current activation as
376 revealed by our screen (Fig. 1i, Supp. Fig. 1d). Interestingly, while H171Azi is inactive without
377 co-expression of STIM1, Orai1 L174Bpa shows UV-induced activation even in the absence of
378 STIM1, as we previously demonstrated in Maltan et al.[26] (Supp. Fig. 1e,f). L174 and the oppo-
379 site residue L261 compose an already known hydrophobic contact essential in STIM1-binding,
380 pore hydration and channel gating [9,23]. Furthermore, also position H171 has been identified as
381 crucial for channel activation, contributing to gating by stabilizing TM3-TM4-contacts [50].

382 To obtain a better understanding of the molecular mechanisms around these residues culmi-
383 nating in a reversed UV-effect, namely UV-induced activation, in contrast to the observed UV-

384 induced current decrease of lower nexus-TM3 UAA-mutants, we mutated residue L261, that is
385 pointing towards TM3, to amino acids of different properties (Fig. 7a).

386 Mutations to glycine, alanine or serine but also to phenylalanine and tryptophan nearly abol-
387 ished STIM1-mediated currents for both Orai1 H171Azi L261G/A/S/F/W and Orai1 L174Bpa
388 L261G/S/F/W. Interestingly, for Orai1 H171Azi L261G/A/S/W and Orai1 L174Bpa L261G/S UV-
389 illumination led to a current increase reaching WT-like or even higher levels, indicating that
390 photocrosslinking restores the communication between the two transmembrane domains, re-
391 spectively (Fig. 7b,c). As exemplarily shown for Orai1 H171Azi L261S, the UV-induced current
392 increase only occurs in the presence and after activation of STIM1, thus, suggesting a confor-
393 mational rearrangement of the upper nexus-TM3 interface after STIM1-binding (Supp. Fig. 8a).

394 For Orai1 H171Azi L261F and Orai1 L174Bpa L261F/W, UV-exposure was unable to signifi-
395 cantly elevate current levels in contrast to Orai1 H171Azi/L174Bpa alone (Fig. 7b,c). Hence,
396 the different size and/or hydrophobicity of L261-mutants seem to interfere with both, STIM1-
397 and UV-induced activation and thus, with the communication within the upper nexus-TM3 in-
398 terface.

399 In contrast, substitutions with either valine or methionine, both rather similar to leucine regard-
400 ing hydrophobicity and size, showed STIM1-mediated current levels nearly comparable to
401 H171Azi/L174Bpa, suggesting that the hydrophobic connection between H171Azi/L174Bpa
402 L261V/M is still intact. Furthermore, a high UV-mediated current increase, to a rather similar
403 level as for Orai1 H171Azi/L174Bpa, was observed, probably stabilizing this interaction by a
404 photocrosslink (Fig. 7b,c).

405 Notably, the UV-mediated current size increased stepwise with increasing amino acid size from
406 the smallest glycine to larger methionine, most similar to leucine regarding size, hydrophobicity
407 and current level. A further increase in size like for L261F/W reverses this trend showing again
408 smaller UV-mediated currents. Thus, the size but also the hydrophobic character of L261
409 seems to be critical for transferring the gating signal from the upper nexus towards the center
410 of the channel complex (Fig. 7b,c). In accord with the critical role of hydrophobicity in the upper
411 nexus-TM3 interface in pore opening, also STIM1-mediated currents of Orai1 L174F L261F
412 were nearly abolished (Sup. Fig. 8b).

413 In addition, we investigated the effect of UV-induced photocrosslinking before STIM1-binding.
414 Here, we observed for both Orai1 H171Azi and Orai1 L174Bpa that UV-illumination directly at
415 the beginning of the whole cell-measurement resulted in a slight UV-mediated current increase
416 with subsequent STIM1-mediated current activation. Orai1 H171Azi reached only WT-like lev-
417 els, in contrast to when UV-illumination occurred after STIM1-binding (Fig. 7d). This suggests
418 that, in particular around H171, conformational changes within the upper nexus-TM3 interface

419 happen after STIM1-binding, which allow enhanced UV-induced activation of Orai1 H171Azi.
420 Orai1 L174Bpa showed only slightly but not significantly reduced current levels when UV-light
421 is applied before STIM1-binding compared to the reverse order of the stimuli (Fig. 7e). Hence,
422 the covalent bond formed between L174Bpa and its potential counterpart in TM4 does not
423 interfere with maximal STIM1-mediated activation. STIM1-binding to Orai1 H171Azi and Orai1
424 L174Bpa remained unaffected of the order of store-depletion and UV-induced crosslinking in
425 FRET experiments (Fig. 7f,g).

426 To summarize, a hydrophobic gating interaction in the upper nexus-TM3 interface
427 (H171/L174/L261) is essential for proper STIM1-mediated currents, as mutations of amino ac-
428 ids with different hydrophobicity and/or size diminish pore opening. UV-mediated photocross-
429 linking can restore this interaction leading to strongly increased currents.

430 **Discussion**

431 In this study, we report that the lower nexus-TM3 interface, which connects the Orai1 C-termi-
432 nus, the major STIM1-binding site[14], to the channel subunit, undergoes a conformational
433 change involving its widening and contributes to proper STIM1-coupling allowing pore opening.
434 These dynamics and interactions likely affect downstream key sites, such as the upper nexus-
435 TM3 as well as the TM3/4-interface, contributing to the transmission of the STIM1-induced
436 activation signal from the C-terminus[7,13] to the inner core of the channel, the pore. Here, our
437 multifaceted experimental approach, combining conventional site-directed mutagenesis, incor-
438 poration of photocrosslinking UAAs, chemically crosslinking UAAs, and reversible cysteine
439 crosslinking experiments, allowed us to gain robust insights into critical interaction partners
440 and patterns as well as steric requirements in the nexus-TM3 interface that trigger STIM1-
441 mediated pore opening [17,44].

442 The incorporation of UAAs enables us to overcome limitations of conventional mutagenesis by
443 transferring novel physicochemical properties to individual amino acids. Photocrosslinking
444 UAAs offer the unique opportunity to study the dynamics of structure-function relationships and
445 site-specific conformational rearrangements, as demonstrated by our previous studies [26]. Yet,
446 Azi exhibits lower photochemical specificity and stability than Bpa, which can lead to unspecific
447 reactions such as ring expansion upon UV-illumination, potentially introducing steric effects, or
448 interactions with membrane lipids [51–53]. To circumvent this issue, we further implemented
449 chemical crosslinking UAAs, enabling to map crosslinking partners[29]. As our experimental data
450 showed robust and reproducible UV-induced effects, which occurred in the presence, but not
451 or distinctly in the absence of STIM1, and are further in line with chemical and cysteine cross-
452 linking experiments, we suggest that non-specific UV-induced crosslinking is unlikely to ac-
453 count for the observed functional outcomes. Notably, the most prominent effects are observed

454 with Azi rather than Bpa, likely because Azi's smaller size allows it to better adapt to the sur-
455 roundings within the nexus-TM3 interface.

456 The results of our different mutagenesis approaches all consistently indicate that a widening
457 of the nexus-TM3 interface leads to pore opening. On the one hand, this is supported by the
458 higher STIM1-induced current densities after incorporation of a bulky amino acid, either a pho-
459 tocrosslinking UAA or an aromatic amino acid, in particular at K265. On the other hand, cross-
460 linking (photo-, chemical, cysteine crosslinking) at certain positions at the nexus-TM3 interface
461 leads to a reduction in STIM1-mediated current densities. While alanine-substitutions only at
462 some sites reduce store-operated current activation, either due to narrowing of the nexus-TM3
463 interface and/or reduced STIM1-coupling, UV-light triggers current reduction to WT- or even
464 smaller levels. Overall, this indicates that crosslinking decreases the nexus-TM3 distance, and
465 our crosslinking assays, in particular chemical and cysteine crosslinking, enabled us to map a
466 contact area contributing to the maintenance of the closed state. In turn, these findings suggest
467 that STIM1 can cause a widening of this interface to trigger signaling to pore opening. In sup-
468 port, GoF-mutants containing the UAA mutation at critical sites in the nexus-TM3 interface (e.g.
469 K265) do not respond to UV-light, likely due to a GoF-mutation-induced conformational
470 change, such as widening, at the nexus-TM3 interface that distances potential crosslinking
471 partners from each other. Our observed slight tendency for UV-induced current reduction in
472 the presence of STIM1 (e.g. of Orai1 K265Azi V181K) suggests some STIM1-induced struc-
473 tural rearrangements, although the open conformation is already set. This supports previous
474 evidence that STIM1-binding fine-tunes pore opening [38]. Under physiological conditions, the
475 widening of the nexus-TM3 interface could be caused by the bending of the nexus node (aa
476 261-265) after STIM1-binding. These findings are in line with previous reports showing that
477 STIM1-binding and/or pore opening are linked to conformational changes of the C-terminus
478 [9,14,15]. Furthermore, our previous studies demonstrate that the TM3-TM4 interface in particular
479 around the V181 position and directly connected to the nexus-TM3 interface undergoes wid-
480 ening to induce pore opening [25,37]. Hence, it is tempting to speculate that the signal of STIM1-
481 binding is transmitted via the nexus-TM3- to the TM4-TM3 interface, which triggers further
482 transmission to the center of channel complex.
483
484 Beyond the widening of the nexus-TM3 interface, additional conformational rearrangements
485 may still occur. In contrast to Orai1 R167Azi, Orai1 H171Azi, and Orai1 K265Azi, which exhibit
486 reduced maximal currents when UV-light is applied prior to STIM1-coupling, Orai1 L174Bpa
487 demonstrates nearly comparable currents regardless of the order in which these stimuli are
488 applied. The fact that the putative UV-induced crosslink formation of L174Bpa with TM4 still

489 permits high current activation suggests that STIM1, in addition to inducing a widening of the
490 nexus-TM3 interface, may also trigger other structural rearrangements.
491
492 While the incorporation of the photocrosslinking UAA at K265 and R167 or an aromatic amino
493 acid at K265 in the nexus resulted in significantly increased currents, store-operated currents
494 of other canonical substitutions of different properties at R167 showed no side-chain depend-
495 ence. A possible reason could be that R167 is not directly pointing towards the nexus but rather
496 pointing slightly out of the nexus-TM3 interface as revealed by investigations of the hOrai1
497 homology model (Fig. 3a) as well as our hOrai1 MD simulations[25] (Supp. Fig. 5b). Hence,
498 changes of the amino acid size of position 167 does not directly influence the distance in the
499 respective interface.

500 Several of our results hint on a potential role of the nexus-TM3 interface in STIM1-coupling.
501 While several aromatic substitutions enhanced STIM1-mediated Orai1 currents, others (e.g.
502 K265W, R167F K265F) did not strongly or not at all enhance STIM1-induced currents. FRET
503 experiments showed that R167Y K265Y exhibits reduced STIM1-coupling. This result is in
504 accord with our previous report, in which we demonstrated impaired STIM1-coupling for some
505 constitutively active Orai1 mutations located at the TM3-TM4 interface [37] (Fröhlich et al. un-
506 published). Heterogenous effects of various A-substitutions in UAA-containing Orai1 mutants
507 cannot only be attributed to changes along the nexus-TM3 interface but could potentially also
508 affect STIM1-coupling. Indeed, several A-substitutions (E166A, E166A R167A, E166A R170A)
509 in Orai1 K265Azi reduced STIM1-coupling. Furthermore, our findings point to a critical impact
510 of charges within this interface in the STIM1-mediated activation. The insertion of reversed
511 charges (E166, K265) or alanine (E166) resulted in reduced STIM1-mediated currents for mul-
512 tiple single or double mutants probably due to strengthened or weakened electrostatic interac-
513 tions. For Orai1 K265E R167E/R170E even STIM1-Orai1 binding was negatively affected.
514 Hence, charges within the nexus-TM3 interface play a critical role in fine-tuning STIM1-cou-
515 pling and pore opening. It remains unclear whether these charges in the nexus-TM3 interface
516 affect STIM1-binding directly or indirectly. As cysteine crosslinking of E166C and K265C works
517 in the STIM1-bound state, we suggest a more indirect effect of the charges on STIM1-binding.

518 Taking a closer look on the structure reveals that at least in three subunits K265 and E166
519 point to each other (Supp. Fig. 5a,9). Thus, crosslinking of at least three subunits leads to
520 robust current reduction. However, it is tempting to speculate that STIM1-binding triggers a
521 reorientation leading to more E166-K265 pairs pointing to each other, thus making up robust
522 crosslinking induced functional effects. However, this requires further proof by a structural res-
523 olution of STIM1 and Orai1 in complex. In addition to cysteine crosslinking induced current
524 reduction of Orai1 E166C K265C, we previously demonstrated that also Orai1 K78C E166C

525 shows diamide-induced current reduction [54]. The reason for this could be that at least in three
526 subunits both, E166 and K265 point also to K78 (Supp. Fig. 5a). Moreover, these findings
527 indicate that changes in charges in this area can affect the local surroundings and conse-
528 quently impact STIM1-coupling and -mediated activation. Moreover, Orai1 E166C could be
529 activated by crosslinking with STIM1 L402C[55], supporting the critical role of E166 and its envi-
530 ronment in STIM1-coupling.

531 Our primary screen of the nexus-TM3 interface revealed two UAA-mutants in the upper nexus
532 (H171Azi, L174Bpa) showing STIM1-mediated activation followed by strong UV-induced cur-
533 rent activation (Fig. 1i, Supp. Fig. 1d). Both STIM1-mediated and UV-induced activation de-
534 pend on the amino acid properties at position 261. While small or aromatic amino acids allow
535 no or only weak store-operated activation, amino acids (V, M) with similar size/hydrophobicity
536 like leucine show WT-like STIM1-mediated current levels. This indicates that hydrophobic in-
537 teractions in the upper nexus-TM3 interface are crucial for maintaining the closed state but
538 also for STIM1-induced activation. In line with the role of hydrophobicity in the upper nexus,
539 two phenylalanines at L174 and L261 abolish STIM1-mediated activation. In accord with our
540 results, other contact pairs close to the nexus-TM3 interface (F178-F257[17], A175-Y258[50]) have
541 been reported to play a critical role in the pore opening mechanism.

542 UV-induced currents of both Orai1 H171Azi and Orai1 L174Bpa correlate with an increase in
543 side-chain size at position 261 in accord with our observations that widening of the nexus-TM3
544 and the TM3-TM4 interfaces contributes to pore opening. Only aromatic amino acids (F, W) at
545 261 do not allow strong UV-induced activation, potentially due to steric hindrance or hydropho-
546 bic interactions generally impairing activation. A covalent interaction formed starting from H171
547 seems to stabilize the open state, which is in accord with our previous finding on the critical
548 role of the TM3-TM4 interface in Orai1 pore opening [25].

549 Interestingly, in the absence of STIM1, Orai1 L174Bpa, but not H171Azi showed UV-induced
550 activation. Taking a closer look at the closed state Orai1 structure reveals that L174Bpa is
551 always opposite S260/L261 in TM4, while H171 is pointing out of the nexus-TM3 interface or
552 to the C-terminus (Supp. Fig. 5c,9). UV-induced current enhancements after maximal STIM1-
553 induced activation of Orai1 H171Azi points to a STIM1-binding induced structural rearrange-
554 ment of C-terminus and TM4 potentially making residues in TM4 accessible for photocross-
555 linking. This behaviour is reflected by corresponding double mutants containing L261 mutated
556 to amino acids with different properties. Interestingly, the open state structure indicates that
557 H171 might still be oriented outward of the nexus-TM3 interface (Supp. Fig. 9), which is in
558 contradiction to our experimental data, and highlights the need for structural resolution of
559 STIM1 complexed with Orai1.

560 In summary, we discovered that the nexus-TM3 interface plays a critical role in the STIM1-
561 mediated pore opening process of Orai1. With the use of photocrosslinking and chemical
562 crosslinking UAAs as well as site-directed mutagenesis, we showed that a widening of the
563 lower nexus-TM3 interface is essential for proper channel activation by STIM1. Furthermore,
564 the contacts formed at the upper nexus-TM3 interface are necessary for signal transduction
565 and pore opening. Our experiments support the findings of Zhou et al.[23] that the binding of
566 STIM1 to the Orai1 C-terminus results in the flexion of the lower nexus, thus inducing a wid-
567 ening of the nexus-TM3 interface. This conformational rearrangement further enables the for-
568 mation of gating interactions in the upper nexus-TM3 interface, that stabilize the opening con-
569 formation of Orai1 and transfer the opening signal towards the more central TM-domains.
570 Along with this, the inner TM3-TM4-TM2´ interface widens, as we discovered in our previous
571 publication[25], thus transmitting the opening signal towards the central pore of the channel. Our
572 studies provide a further basis for continuing studies of our previous findings[33] on the role of
573 isoform-specific features of the TM3-TM4 interfaces in fine-tuning Orai pore opening.

574 Elucidating the precise conformational dynamics during STIM1-mediated Orai1 activation re-
575 mains a fundamental challenge in the field. Here, we uncover key mechanistic principles gov-
576 erning pore opening by combining site-specific photo- and chemical crosslinking with conven-
577 tional mutagenesis. The discovered results gained by different approaches are all in line and
578 supporting the critical role of the nexus-TM3 interface in pore opening and supplement previ-
579 ous important findings [23,25,50]. This study again highlights how the use of unnatural amino acids
580 is suitable to uncover novel CRAC channel dynamics. Our innovative methods facilitate the
581 detailed discovery of conformational events happening during pore opening at amino acid
582 level, thus opening new possibilities of future drug design and therapeutic strategies.

583

584 **Methods**

585

586 **Molecular biology**

587 For C-terminal fluorescent labeling of human Orai1 (accession number NM_032790; provided
588 by A. Rao's laboratory), the gene was cloned into the pEYFP-N1 expression vector (Clontech)
589 using XhoI and BamHI restriction sites. Site-directed mutagenesis and amber stop codon
590 (TAG) insertion for site-specific UAA-incorporation were carried out using the QuikChange™
591 XL kit (Stratagene), with the corresponding Orai1 construct as a template. Corresponding Pri-
592 mer sequences were purchased from Eurofins Genomics. Human STIM1 (accession number
593 NM_003156), N-terminally tagged with ECFP, was kindly provided by T. Meyer (Stanford Uni-
594 versity). STIM1 point mutations were introduced using the QuikChange™ XL kit as well. All
595 constructs were verified by DNA sequencing (Eurofins Genomics/Microsynth).

596 Humanized aminoacyl-tRNA synthetase/tRNA pairs for the recognition of unnatural amino ac-
597 ids azido-L-phenylalanine, benzoyl-L-phenylalanine and BC_nY were purchased from Addgene
598 (#105829, #155342 and #155343).

599 **Cell culture and transfection**

600 Human embryonic kidney 293 -T (HEK293-T) cells (#ACC635, DSMZ) were cultured in DMEM,
601 supplemented with L-glutamine (2mM), streptomycin (100µg/ ml), penicillin (100 units/ml) and
602 10% fetal calf serum at 37°C in a humidity-controlled incubator with 5% CO_2.

603 Transient transfection of HEK293-T cells was performed using TransFectin™ Lipid Reagent
604 (Bio-Rad; 2.5 µL per transfection). Standard plasmid ratios were 1 µg Orai1: 2 µg tRNA/aaRS;
605 1 µg STIM1 for co-expression. Experiments were conducted 24 h post-transfection in wild-type
606 HEK293-T.

607 Throughout all experiments, wild-type or mutant Orai1-YFP constructs were used, along with
608 STIM1-CFP where applicable. Media of transfected cells was supplemented with 1 mM photo-
609 crosslinking unnatural amino acids (azido-L-phenylalanine or benzoyl-L-phenylalanine;
610 BACHEM, dissolved in 0.5 M NaOH) and 0.3 mM chemical crosslinking unnatural amino acids
611 (BC_nY, synthesized by our collaboration partner M. Waser according to Xiang et al.[39], dissolved
612 in DMSO). Mycoplasma contamination was routinely tested using the VenorGeM Advanced
613 Mycoplasma Detection Kit (Minerva Biolabs).

614

615 **Electrophysiology**

616 Electrophysiological recordings were performed using an inverted microscope (Zeiss Axiovert
617 200), an Axopatch 200B amplifier (Molecular Devices), a PatchStar micromanipulator (Scien-
618 tifica), and a Lumencor Spectra III light engine. Electrophysiological records were acquired
619 with pClamp11 software. 2.2 mW/cm² UV-intensity was used within all experiments. Whole-
620 cell patch-clamp recordings were conducted at room temperature (20°C) using an Ag/AgCl
621 reference electrode. Cells, grown in petri dishes were reseeded onto poly-L-lysine-coated co-
622 verslips 4 h to 18 h post-transfection in medium containing 0.1 mM Ca^{2+} and used for meas-
623 urements 6–10 h later. For time-course and I/V measurements, voltage ramps from –90 mV to
624 +90 mV over 1 s were applied every 5 s starting from a holding potential of 0 mV. Fast Ca^{2+}-
625 dependent inactivation (FCDI) was assessed using voltage steps to –70, –90, or –110 mV for
626 2000 ms starting from a holding potential of 0 mV.

627 Passive store-depletion was triggered via the internal pipette solution containing (in mM): 145
628 Cs-methane sulfonate, 20 EGTA, 10 HEPES, 8 NaCl, 3.5 $MgCl_2$, pH 7.2. The standard extra-
629 cellular solution contained (in mM): 145 NaCl, 10 HEPES, 10 $CaCl_2$, 10 glucose, 5 CsCl, 1
630 $MgCl_2$, pH 7.4. For cysteine crosslinking experiments 1 mL of a 1 mM Diamide in 10 mM Ca^{2+}
631 solution was used for disulfide bond formation and 1 mL of a 5 mM BMS (Bis(2- mercap-
632 toethyl)sulfone) in 10 mM Ca^{2+} solution was used for bond-cleavage. Solution exchange during
633 the experiment was performed using a Thomas Wisa perfusion pump.

634 Applied voltages were not corrected for the liquid junction potential, which was determined as
635 +12mV. Leak currents were subtracted either from initial baseline traces after whole-cell break-
636 in or from 10 µM La^{3+}-blocked traces at the end of the experiment.

637 **Confocal FRET Fluorescence Microscopy**

638 Confocal FRET imaging was performed at room temperature (20°C) 18–24 h after transfection.
639 The standard extracellular solution containing (in mM): 145 NaCl, 5 KCl, 10 HEPES, 10 glu-
640 cose, 1 $MgCl_2$, 2 $CaCl_2$, pH 7.4. For Ca^{2+} store-depletion, a Ca^{2+}-free extracellular solution
641 containing 1 µM Thapsigargin was used. Imaging was conducted using a CSU-X1 real-time
642 confocal system (Yokogawa Electric Corporation, Japan) equipped with two CoolSNAP HQ2
643 CCD cameras (Photometrics, AZ, USA), a dual-port adapter dichroic, 505lp; cyan emission
644 filter, 470/24; yellow emission filter, 535/30; Chroma Technology Corporation, VT, USA), and
645 two diode lasers (445 nm and 515 nm; Visitron Systems). The system was mounted on an Axio
646 Observer.Z1 inverted microscope (Carl Zeiss) and placed on an anti-vibration table (Vision
647 IsoStation, Newport). A Thomas Wisa perfusion pump enabled continuous extracellular

solution exchange during the experiment. Image acquisition and system control were carried out via the VisiView software (v2.1.4, Visitron Systems). The illumination times for individual sets of images (CFP, YFP, FRET) that were recorded consecutively with a minimum delay were kept in a range of 100–300 ms. To account for spectral bleed-through and cross-excitation, correction factors for YFP cross-excitation (α) and CFP crosstalk (β) were determined daily using control samples expressing only CFP or YFP. FRET analysis was limited to pixels with CFP:YFP ratios between 0.1:10 and 10:0.1. After this threshold determination as well as background signal subtraction, the apparent FRET efficiency E_{app} was calculated on a pixel-to-pixel basis using a custom MATLAB routine (v7.11.0, MathWorks, Inc., MA, USA) and the following equation:

$$E_{app} = \frac{I_{FRET} - aI_{YFP} - bI_{CFP}}{I_{FRET} - aI_{YFP} + (G - b)I_{CFP}}$$

where I_{FRET}, I_{YFP} and I_{CFP} denote the intensities of the FRET, YFP and CFP images, respectively. G denotes a microscope-specific constant parameter that was experimentally determined as 2.75 [9,19].

Molecular Modeling and structural analysis

We retrieved the all-atom homology model of hOrai1 published by Frischauf et al.[48] from the model archive with accession code "ma-akdjp" [56]. We defined the transmembrane region by focusing on the average z-coordinate of the R91 alpha carbon in all monomers at the cytosolic mouth of the Orai1 pore. From this point, we defined a membrane vector in z-direction with 3 nm length. This slab domain will be treated as an implicit membrane with $\varepsilon_r = 2$ throughout our MC-PBE approach [44–46]. The protein domain was defined by its enveloping Connolly surface, which is generated by rolling a spherical water probe with a radius of 0.14 nm over the Van-der-Waals surface of hOrai1 [57]. The aqueous environment is modelled with a dielectric constant $\varepsilon_r = 80$, the protein itself with $\varepsilon_r = 4$. We defined the Debye length of our system with about 0.8 nm by providing a physiological concentration of monovalent ions 0.15 M in our aqueous domain at a temperature of 300 K [58]. In our next step, we aim at the numerical solution of the linearised Poisson-Boltzmann equation using TAPBS[46] on a simple cubic grid for every titratable side chain in isolation and, separately, in its native protein environment. Starting from a coarse grid with 16.1 nm edge length and a grid constant of 0.3 nm, we obtained our final data from a calculation on a grid with a grid constant of 0.025 nm using the same edge length. By virtue of a thermodynamic cycle analysis[47], we can infer the change of Gibbs free energy due to protonation of a single side chain in the protein. We use these Gibbs free energies to perform a Monte-Carlo simulation using the Metropolis-Hastings algorithm[59] implemented in Karlsberg 2[45] to obtain an optimal protonation pattern in the canonical ensemble of the hOrai1 channel between pH 5 and pH 9 at 300 K. These patterns are defined by microscopic protonation probabilities of single titratable side chains, which can be used to assess the preferred

683 titration states and effective pKa values of K78, E166, K265, R167, H264 in all hOrai1 monomers
684 at pH 7.

685 To control and compare our findings from the MC-PBE approach, we started an independent anal-
686 ysis of effective pKa values in hOrai1 with PROPKA3[42,43] using the code provided on the GitHub
687 repository[60] and pre-defined standard settings with the very same homology model structure [48,56].
688 We provide the PROPKA3 output as Supplementary File 1.

689 Structural analyses were performed on published molecular dynamics trajectories of the homology
690 model of Orai1 WT based of the closed dOrai X-ray structure [61]. Our distance measurements were
691 carried out on random samples from the equilibrated trajectory parts. Snapshot number 122 was
692 used for the structural analysis carried out in Supp. Fig. 5.

693 **Statistics and Reproducibility**

694 Data are presented as mean ± SEM, with (n) indicating the number of independent experi-
695 ments. For statistical comparison between two independent groups, the Mann–Whitney test
696 was applied, with $p < 0.05$ considered statistically significant. Variance homogeneity was as-
697 sessed using Levene's test. If the assumption was fulfilled, one-way ANOVA test was used for
698 the statistical comparison of multiple independent samples using the F-distribution, followed
699 by Fisher's least significant difference (LSD) post hoc test. If the assumption was not fulfilled,
700 Welch's ANOVA followed by Games–Howell post hoc test was used. Normality of the data was
701 verified using the Shapiro–Wilk test or, alternatively, the one-sample Kolmogorov–Smirnov
702 test. All corresponding *F* and *p* values for the Main Figures are listed in Supplementary Table
703 1.

704 All experiments were carried out at least on two different days in paired comparisons leading
705 to similar results. Cell images were taken for each experiment showing comparable cellular
706 distribution of the respective proteins/mutants, as shown in one representative image in the
707 respective figures.

708 **Data Availability**

709 Source data will be uploaded to zenodo upon acceptance.

Acknowledgements

We thank S. Buchegger for excellent technical assistance. We thank C.Humer for critically proofreading the manuscript. This research was funded by the Austrian Science Fund (FWF) projects [doi:10.55776/P32851], [doi:10.55776/ P35900] and [doi:10.55776/P36202] to I.D and [doi:10.55776/PAT 6871323] to A.T. For open access purposes, the author has applied a CC BY public copyright license to any author-accepted manuscript version arising from this submission.

Conflict of Interest

The authors declare no competing interests.

Author contributions

JS and ID conceived and coordinated the study and wrote the paper. JS, HN, and TR performed and analyzed electrophysiological experiments. MP, AS carried out fluorescence microscopy experiments. JS, YN, SH, MF, DT contributed to molecular biology. VA, SW, HK performed and supervised computational studies. CM, WN and MW synthesized chemical crosslinking UAAs. All authors reviewed the results and approved the final version of the manuscript.

Supplementary information

includes 9 Supplementary Figures (Supp. Fig. 1-9), 1 Supplementary Table and 1 Supplementary File.

Supplementary Figure 1: UV-triggered inhibition of Orai1 currents via photocrosslinking UAAs introduced in the nexus and in TM3 is dependent on the presence of STIM1.

Supplementary Figure 2: Alanine substitutions in TM3 opposite to the nexus-UAA do not prevent UV-induced current inhibition, but affect STIM1-mediated activation.

Supplementary Figure 3: Constitutively active Orai1 mutations interfere with UV-induced current inhibition upon UAA-insertion at the nexus–TM3 interface.

Supplementary Figure 4: Photo- and chemical crosslinking at the nexus–TM3 interface restricts STIM1-mediated channel opening.

Supplementary Figure 5: Orientation of key residues in the nexus-TM3 interface is critical for UV-induced photocrosslinking.

741 Supplementary Figure 6: Titration states of E166, R167, H264 and K265 based on the closed
742 state of Orai1.

743 Supplementary Figure 7: Charged residues along the nexus-TM3 interface are required for
744 STIM1-mediated Orai1 channel gating.

745 Supplementary Figure 8: Interactions in the upper hydrophobic nexus-TM3 interface are es-
746 sential for STIM1-mediated Orai1 pore opening.

747 Supplementary Figure 9: The channel conformation of the nexus-TM3 interface of the closed
748 and the open state of Orai1.

749 Supplementary Table 1: Results of statistical tests.

750 Supplementary File 1: Results of effective pKa values in hOrai1.

751 **References**

752 1. Emrich, S. M., Yoast, R. E. & Trebak, M. Physiological Functions of CRAC Channels. *Annu Rev*
753 *Physiol* **84**, 355–379 (2022).

754 2. Berridge, M. J., Lipp, P. & Bootman, M. D. The versatility and universality of calcium signalling.
755 *Nat Rev Mol Cell Biol* **1**, 11–21 (2000).

756 3. Prakriya, M. & Lewis, R. S. Store-Operated Calcium Channels. *Physiol Rev* **95**, 1383–1436 (2015).

757 4. Prakriya, M. *et al.* Orai1 is an essential pore subunit of the CRAC channel. *Nature* **443**, 230–233
758 (2006).

759 5. Liou, J. *et al.* STIM is a Ca2+ sensor essential for Ca2+-store- depletion-triggered Ca2+ influx.
760 *Current Biology* **15**, 1235–1241 (2005).

761 6. Zhang, S. L. *et al.* STIM1 is a Ca2+ sensor that activates CRAC channels and migrates from the
762 Ca2+ store to the plasma membrane. *Nature* **437**, 902–905 (2005).

763 7. Feske, S. *et al.* A mutation in Orai1 causes immune deficiency by abrogating CRAC channel func-
764 tion. *Nature* **441**, 179–185 (2006).

765 8. Fahrner, M. *et al.* A coiled-coil clamp controls both conformation and clustering of stromal in-
766 teraction molecule 1 (STIM1). *J Biol Chem* **289**, 33231–33244 (2014).

767 9. Tiffner, A., Maltan, L., Weiss, S. & Derler, I. The Orai Pore Opening Mechanism. *Int J Mol Sci* **22**,
768 (2021).

769 10. Sallinger, M. *et al.* Activation mechanisms and structural dynamics of STIM proteins. *J Physiol*
770 (2023) doi:10.1113/JP283828.

771 11. Feske, S. CRAC channels and disease – From human CRAC channelopathies and animal models
772 to novel drugs. *Cell Calcium* vol. 80 112–116 Preprint at
773 https://doi.org/10.1016/j.ceca.2019.03.004 (2019).

774 12. Tiffner, A. *et al.* CRAC channel opening is determined by a series of Orai1 gating checkpoints in
775 the transmembrane and cytosolic regions. *J Biol Chem* (2020) doi:10.1074/jbc.RA120.015548.

776 13. Lacruz, R. S. & Feske, S. Diseases caused by mutations in ORAI1 and STIM1. *Ann N Y Acad Sci*
777 **1356**, 45–79 (2015).

778 14. Hou, X., Pedi, L., Diver, M. M. & Long, S. B. Crystal structure of the calcium release-activated
779 calcium channel orai. *Science (1979)* **338**, 1308–1313 (2012).

780 15. Hou, X., Outhwaite, I. R., Pedi, L. & Long, S. B. Cryo-em structure of the calcium release-activated
781 calcium channel orai in an open conformation. *Elife* **9**, 1–27 (2020).

782 16. Hou, X., Burstein, S. R. & Long, S. B. Structures reveal opening of the store-operated calcium
783 channel Orai. *Elife* **7**, (2018).

784 17. Liu, X. *et al.* Molecular understanding of calcium permeation through the open Orai channel.
785 *PLoS Biol* **17**, e3000096 (2019).

786 18. Muik, M. *et al.* Dynamic coupling of the putative coiled-coil domain of ORAI1 with STIM1 medi-
787 ates ORAI1 channel activation. *J Biol Chem* **283**, 8014–8022 (2008).

19. Park, C. Y. *et al.* STIM1 clusters and activates CRAC channels via direct binding of a cytosolic domain to Orai1. *Cell* **136**, 876–890 (2009).

20. Li, Z. *et al.* Mapping the interacting domains of STIM1 and Orai1 in Ca2+ release-activated Ca2+ channel activation. *J Biol Chem* **282**, 29448–29456 (2007).

21. Butorac, C., Krizova, A. & Derler, I. Structure and activation mechanisms of CRAC channels. *Adv Exp Med Biol* **in press**, (2018).

22. Fahrner, M., Grabmayr, H. & Romanin, C. Mechanism of STIM activation. *Curr Opin Physiol* 74–79 (2020).

23. Zhou, Y. *et al.* The STIM1-binding site nexus remotely controls Orai1 channel gating. *Nat Commun* **7**, 13725 (2016).

24. Tirado-Lee, L., Yamashita, M. & Prakriya, M. Conformational Changes in the Orai1 C-Terminus Evoked by STIM1 Binding. *PLoS One* **10**, e0128622 (2015).

25. Najjar, H. *et al.* STIM1-induced widening of non-pore-lining TM interfaces is crucial for Orai1 pore opening. *Cell Rep Phys Sci* 102623 (2025) doi:10.1016/j.xcrp.2025.102623.

26. Maltan, L. *et al.* Photocrosslinking-induced CRAC channel-like Orai1 activation independent of STIM1. *Nat Commun* **14**, 1286 (2023).

27. Klippenstein, V., Mony, L. & Paoletti, P. Probing Ion Channel Structure and Function Using Light-Sensitive Amino Acids. *Trends Biochem Sci* **43**, 436–451 (2018).

28. Nodling, A. R., Spear, L. A., Williams, T. L., Luk, L. Y. P. & Tsai, Y. H. Using genetically incorporated unnatural amino acids to control protein functions in mammalian cells. *Essays Biochem* **63**, 237–266 (2019).

29. Coin, I. Application of non-canonical crosslinking amino acids to study protein–protein interactions in live cells. *Curr Opin Chem Biol* **46**, 156–163 (2018).

30. Nguyen, T.-A., Cigler, M. & Lang, K. Expanding the Genetic Code to Study Protein-Protein Interactions. *Angewandte Chemie International Edition* **57**, 14350–14361 (2018).

31. Cai, X. *et al.* Pore properties of Orai1 calcium channel dimers and their activation by the STIM1 ER calcium sensor. *Journal of Biological Chemistry* **293**, 12962–12974 (2018).

32. Frischauf, I. *et al.* Transmembrane helix connectivity in Orai1 controls two gates for calcium-dependent transcription. *Sci Signal* **10**, (2017).

33. Tiffner, A. *et al.* Transmembrane Domain 3 (TM3) Governs Orai1 and Orai3 Pore Opening in an Isoform-Specific Manner. *Front Cell Dev Biol* **9**, (2021).

34. McNally, B. A., Somasundaram, A., Yamashita, M. & Prakriya, M. Gated regulation of CRAC channel ion selectivity by STIM1. *Nature* **482**, 241–245 (2012).

35. Yamashita, M. *et al.* The basic residues in the Orai1 channel inner pore promote opening of the outer hydrophobic gate. *Journal of General Physiology* **152**, 1–14 (2020).

36. Yeung, P. S. W. *et al.* Mapping the functional anatomy of Orai1 transmembrane domains for CRAC channel gating. *Proc Natl Acad Sci U S A* **115**, E5193–E5202 (2018).

37. Hopl, V. *et al.* Water in peripheral TM-interfaces of Orai1-channels triggers pore opening. *Communications Biology 2024 7:1* **7**, 1–16 (2024).

827 38. Krizova, A., Maltan, L. & Derler, I. Critical parameters maintaining authentic CRAC channel hall-
828 marks. *Eur Biophys J* **48**, 425–445 (2019).

829 39. Xiang, Z. *et al.* Proximity-enabled protein crosslinking through genetically encoding haloalkane
830 unnatural amino acids. *Angew Chem Int Ed Engl* **53**, 2190–2193 (2014).

831 40. Hart, H., Craine, L. E., Hart, D. J. & Hadad, C. M. *Organische Chemie*. (WILEY-VCH, Weinheim ,
832 2007).

833 41. Cigler, M. *et al.* Proximity-Triggered Covalent Stabilization of Low-Affinity Protein Complexes In
834 Vitro and In Vivo. *Angewandte Chemie International Edition* **56**, 15737–15741 (2017).

835 42. Søndergaard, C. R., Olsson, M. H. M., Rostkowski, M. & Jensen, J. H. Improved Treatment of
836 Ligands and Coupling Effects in Empirical Calculation and Rationalization of p K_a Values. *J Chem*
837 *Theory Comput* **7**, 2284–2295 (2011).

838 43. Olsson, M. H. M., Søndergaard, C. R., Rostkowski, M. & Jensen, J. H. PROPKA3: Consistent Treat-
839 ment of Internal and Surface Residues in Empirical p K_a Predictions. *J Chem Theory Comput* **7**,
840 525–537 (2011).

841 44. Ullmann, G. M. & Knapp, E.-W. Electrostatic models for computing protonation and redox equi-
842 libria in proteins. *European Biophysics Journal* **28**, 533–551 (1999).

843 45. Rabenstein, B. & Knapp, E.-W. Calculated pH-Dependent Population and Protonation of Carbon-
844 Monoxy-Myoglobin Conformers. *Biophys J* **80**, 1141–1150 (2001).

845 46. Kieseritzky, G. & Knapp, E.-W. Optimizing pKA computation in proteins with pH adapted confor-
846 mations. *Proteins: Structure, Function, and Bioinformatics* **71**, 1335–1348 (2007).

847 47. Renger, T. & Müh, F. Understanding photosynthetic light-harvesting: a bottom up theoretical
848 approach. *Phys. Chem. Chem. Phys.* **15**, 3348–3371 (2013).

849 48. Frischauf, I. *et al.* A calcium-accumulating region, CAR, in the channel Orai1 enhances Ca^{2+} per-
850 meation and SOCE-induced gene transcription. *Sci Signal* **8**, (2015).

851 49. Pace, C. N., Grimsley, G. R. & Scholtz, J. M. Protein Ionizable Groups: pK Values and Their Con-
852 tribution to Protein Stability and Solubility. *Journal of Biological Chemistry* **284**, 13285–13289
853 (2009).

854 50. Augustynek, B. *et al.* Discovery of novel gating checkpoints in the Orai1 calcium channel by sys-
855 tematic analysis of constitutively active mutants of its paralogs and orthologs. *Cell Calcium* **105**,
856 102616 (2022).

857 51. Klippenstein, V., Ghisi, V., Wietstruk, M. & Plested, A. J. Photoinactivation of glutamate receptors
858 by genetically encoded unnatural amino acids. *J Neurosci* **34**, 980–991 (2014).

859 52. Tanaka, Y., Bond, M. R. & Kohler, J. J. Photocrosslinkers illuminate interactions in living cells.
860 *Molecular BioSystems* vol. 4 473–480 Preprint at https://doi.org/10.1039/b803218a (2008).

861 53. Grunbeck, A., Huber, T., Sachdev, P. & Sakmar, T. P. Mapping the ligand-binding site on a G pro-
862 tein-coupled receptor (GPCR) using genetically encoded photocrosslinkers. *Biochemistry* **50**,
863 3411–3413 (2011).

864 54. Fahrner, M. *et al.* Communication between N terminus and loop2 tunes Orai activation. *J Biol*
865 *Chem* **293**, 1271–1285 (2018).

55. Butorac, C. *et al.* A novel STIM1-Orai1 gating interface essential for CRAC channel activation. *Cell Calcium* **79**, 57–67 (2019).

56. Rudiger, E. Structure of human Orai1 based on homology with dOrai. https://www.modelarchive.org/doi/10.5452/ma-akdjp (2015) doi:DOI: 10.5452/ma-akdjp.

57. Connolly, M. L. Analytical molecular surface calculation. *J Appl Crystallogr* **16**, 548–558 (1983).

58. Debye, P. & ´Hückel, E. The Theory of Electrolytes I. Lowering of Freezing Point and Related Phenomena. *Physikalische Zeitschrift* **24**, 185–206 (1923).

59. Metropolis, N., Rosenbluth, A. W., Rosenbluth, M. N., Teller, A. H. & Teller, E. Equation of State Calculations by Fast Computing Machines. *J Chem Phys* **21**, 1087–1092 (1953).

60. GitHub Inc. PROPKA 3.0. (2025).

61. Derler, I. *et al.* STIM1-induced widening of non-pore-lining TM interfaces is crucial for Orai1 pore opening . Preprint at https://doi.org/10.5281/zenodo.15021906 (2025).

882

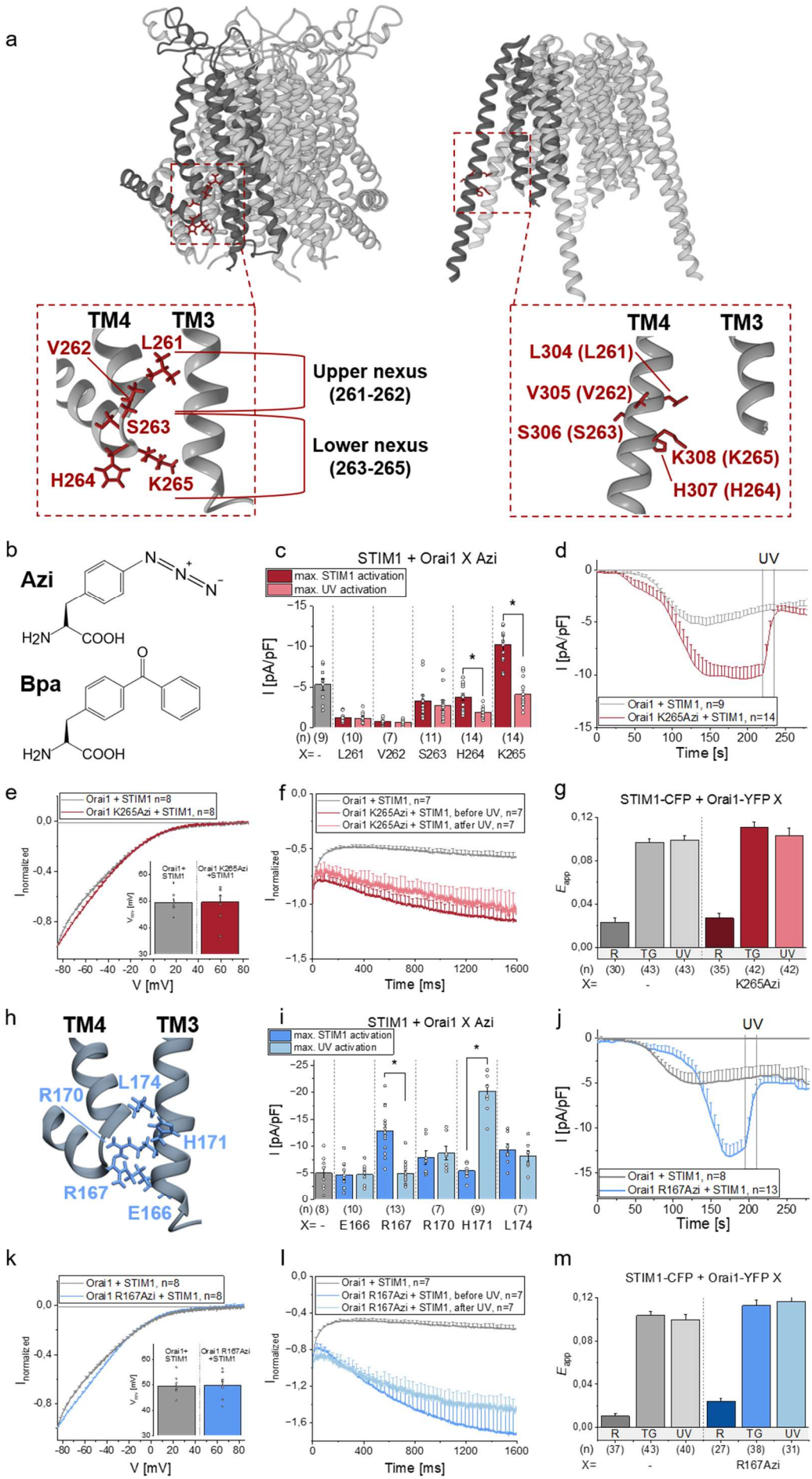
a
TM4
TM3
V262
L261
S263
H264
K265
Upper nexus (261-262)
Lower nexus (263-265)
L304 (L261)
V305 (V262)
S306 (S263)
K308 (K265)
H307 (H264)
b
Azi
Bpa
H2N
COOH
c
STIM1 + Orai1 X Azi
max. STIM1 activation
max. UV activation
I [pA/pF]
(n) (9) (10) (7) (11) (14) (14)
X= - L261 V262 S263 H264 K265
d
UV
Orai1 + STIM1, n=9
Orai1 K265Azi + STIM1, n=14
Time [s]
e
Orai1 + STIM1 n=8
Orai1 K265Azi + STIM1, n=8
V [mV]
f
Orai1 + STIM1, n=7
Orai1 K265Azi + STIM1, before UV, n=7
Orai1 K265Azi + STIM1, atfer UV, n=7
Time [ms]
g
STIM1-CFP + Orai1-YFP X
R TG UV R TG UV
(n) (30) (43) (43) (35) (42) (42)
X= - K265Azi
h
TM4
TM3
R170
L174
H171
R167
E166
i
STIM1 + Orai1 X Azi
max. STIM1 activation
max. UV activation
I [pA/pF]
(n) (8) (10) (13) (7) (9) (7)
X= - E166 R167 R170 H171 L174
j
UV
Orai1 + STIM1, n=8
Orai1 R167Azi + STIM1, n=13
Time [s]
k
Orai1 + STIM1, n=8
Orai1 R167Azi + STIM1, n=8
V [mV]
l
Orai1 + STIM1, n=7
Orai1 R167Azi + STIM1, before UV, n=7
Orai1 R167Azi + STIM1, after UV, n=7
Time [ms]
m
STIM1-CFP + Orai1-YFP X
R TG UV R TG UV
(n) (37) (43) (40) (27) (38) (31)
X= - R167Azi

883 **Figure 1: Photocrosslinking UAAs at sites in the nexus and opposite in TM3 allow upon**
884 **STIM1-mediated activation UV-induced current reduction**

885 **a)** Scheme showing closed hOrai1 (left; PDB: 4HKR) and open dOrai (right; PDB: 6BBF) struc-
886 tures with insets depicting the upper and lower nexus region (LVSHK; 261-265 in hOrai1/ 304-
887 307 in dOrai) with tested residues highlighted in red. Numbers indicate positions in hOrai1 or
888 dOrai with those of hOrai1 in brackets. **b)** Chemical structures of Azi and Bpa. **c) i)** Bar dia-
889 grams showing maximal current densities after STIM1-activation and 15s UV-illumination of c)
890 Orai1 nexus-mutants and i) Orai1 TM3-mutants containing Azi. Statistical significance before
891 and after UV-illumination are indicated by asterisk * ($p< 0.05$). **d) j)** Time course of current
892 densities after whole cell break-in of Orai1 WT and d) Orai1 K265Azi and j) Orai1 R167Azi co-
893 expressed with STIM1. UV-light is applied for 15s (t= 220s (d)/195s (j)), after maximum STIM1-
894 mediated currents have been reached. **e) k)** Normalized I/V relationships of Orai1 WT and e)
895 Orai1 K265Azi and k) Orai1 R167Azi in the presence of STIM1. Inlet represents the reversal
896 potential (V_{rev}) of STIM1-mediated currents. **f) l)** Time course showing normalized currents of
897 Orai1 WT compared to f) Orai1 K265Azi and l) Orai1 R167Azi before and after 15s UV-illumi-
898 nation in the presence of STIM1. Currents were obtained from the application of a voltage step
899 of -110 mV. **g) m)** Bar diagrams exhibiting FRET efficiency (E_{app}) detecting the interaction of
900 STIM1-CFP with Orai1-YFP WT compared to g) Orai1-YFP K265Azi and m) Orai1-YFP
901 R167Azi at resting conditions (R), after store-depletion with 1 µM Thapsigargin (TG) and after
902 60s UV-illumination (UV). **h)** Schematic representation of the nexus-TM3 interface highlighting
903 tested residues in TM3. Data represent mean values ± SEM of indicated number (n) of exper-
904 iments. Single values are indicated as grey circles. Detailed statistic values are shown in Sup-
905 plementary Table 1.

906

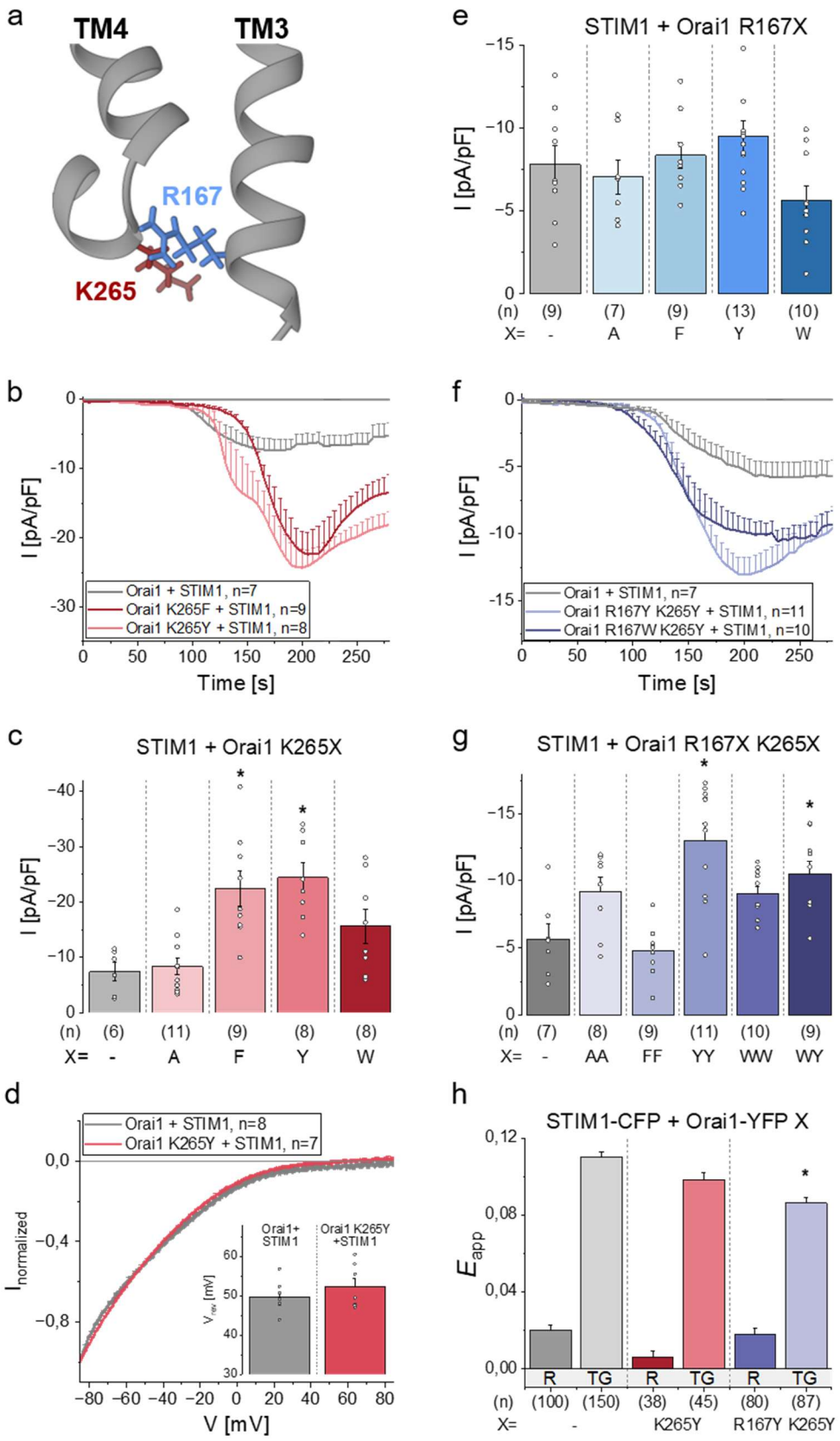

Figure 2: Aromatic substitutions at K265 increase STIM1-mediated currents of Orai1

a) Schematic representation of key residues K265 and R167 in the nexus-TM3 interface of Orai1. **b) f)** Time course of current densities after whole cell break-in of Orai1 WT and b) Orai1

911 K265F/Y and f) Orai1 R167Y K265Y and Orai1 R167W K265Y in the presence of STIM1. **c) e)**
912 **g)** Bar diagrams showing maximal current densities after STIM1-activation of Orai1 WT and c)
913 Orai1 K265A/F/Y/W, e) Orai1 R167A/F/Y/W and g) Orai1 R167A K265A, Orai1 R167F K265F,
914 Orai1 R167W K265W and Orai1 R167W K265Y. Statistical significance of Orai1 mutants com-
915 pared to Orai1 WT are indicated by asterisk * ($p < 0.05$). **d)** Normalized I/V relationships of
916 Orai1 WT and Orai1 K265Y in the presence of STIM1. Inlet represents the reversal potential
917 (V_{rev}) of STIM1-activated Orai1 currents. **h)** Bar diagrams exhibiting the FRET efficiency (E_{app})
918 detecting the interaction of STIM1-CFP with Orai1-YFP WT compared to Orai1-YFP K265Y
919 and Orai1-YFP R167Y K265Y at resting conditions (R) and after store-depletion with 1 µM
920 Thapsigargin (TG). Statistical significance of Orai1 mutants compared to Orai1 WT at similar
921 conditions are indicated as asterisk * ($p < 0.05$). Single values are indicated as grey circles.
922 Data represent mean values ± SEM of indicated number (n) of experiments. Detailed statistic
923 values are shown in Supplementary Table 1.

924

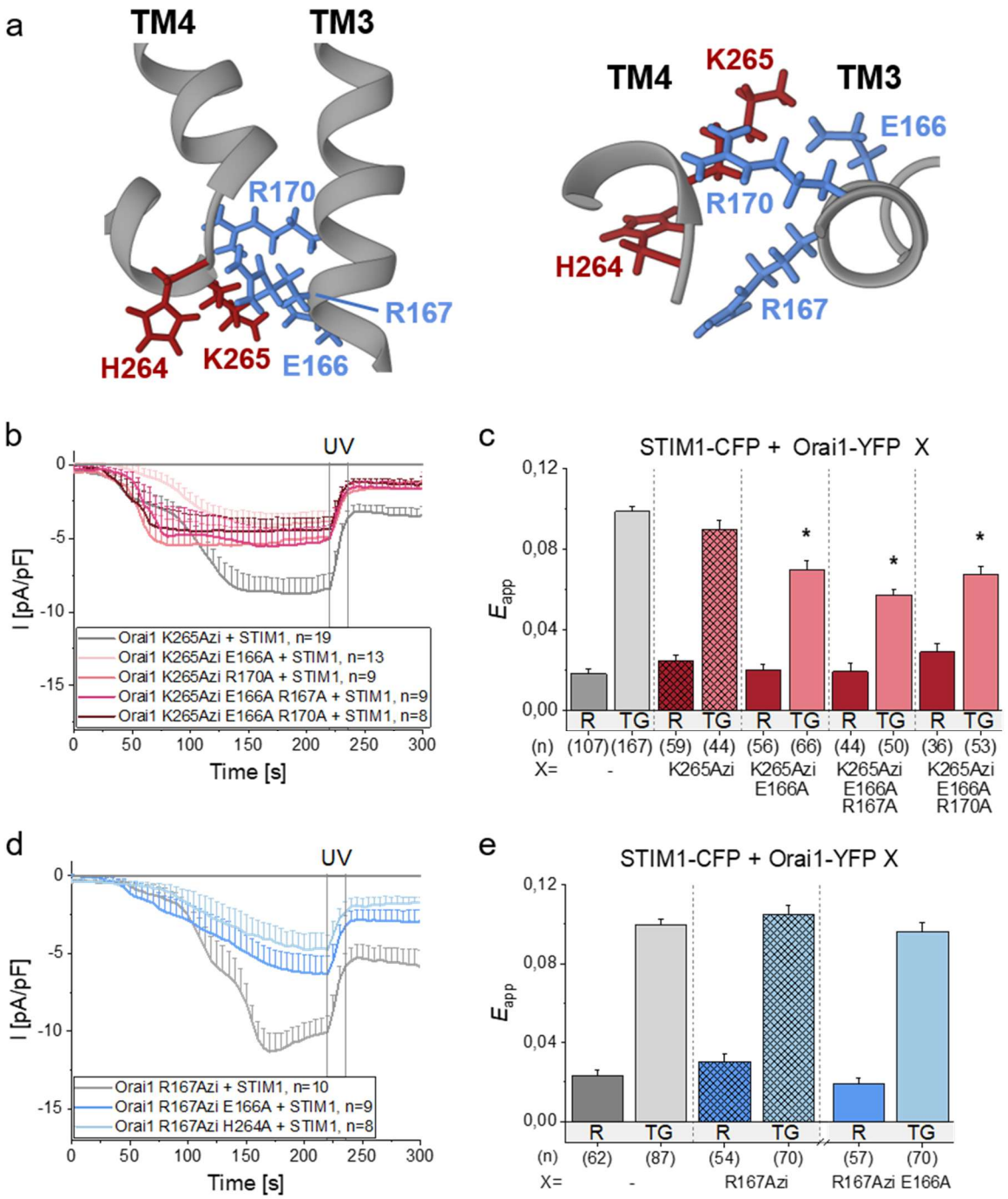

Figure 3: Alanine substitutions in TM3 opposite the UAA in the nexus leave UV-mediated current decrease unaffected, but, in some cases, decrease STIM1-induced maximal activation

a) Schematic representation of the side view (left) and top view (right) of the Orai1 nexus-TM3 interface highlighting key residues. **b) d)** Time course of current densities after whole cell break-in of b) Orai1 K265Azi and Orai1 K265Azi E166A/R170A/E166A R167A/E166A R170A and d) Orai1 R167Azi and Orai1 R167Azi E166A/H264A in the presence of STIM1. UV-light is applied for 15s at t= 220s, after maximum STIM1-mediated currents were reached. **c) e)** Bar

934 diagrams showing FRET efficiency (E_{app}) detecting the binding interaction of STIM1-CFP with
935 Orai1-YFP WT and c) Orai1-YFP K265Azi/ K265Azi E166A/E166A R167A/E166A R170A and
936 e) Orai1-YFP R167Azi/R167Azi E166A at resting conditions (R) and after store-depletion with
937 1 μM Thapsigargin (TG). Statistical significance of Orai1 mutants compared to Orai1 WT at
938 similar conditions are indicated by asterisk * ($p < 0.05$). Data represent mean values ± SEM of
939 indicated number (n) of experiments. Detailed statistic values are shown in Supplementary
940 Table 1.

941

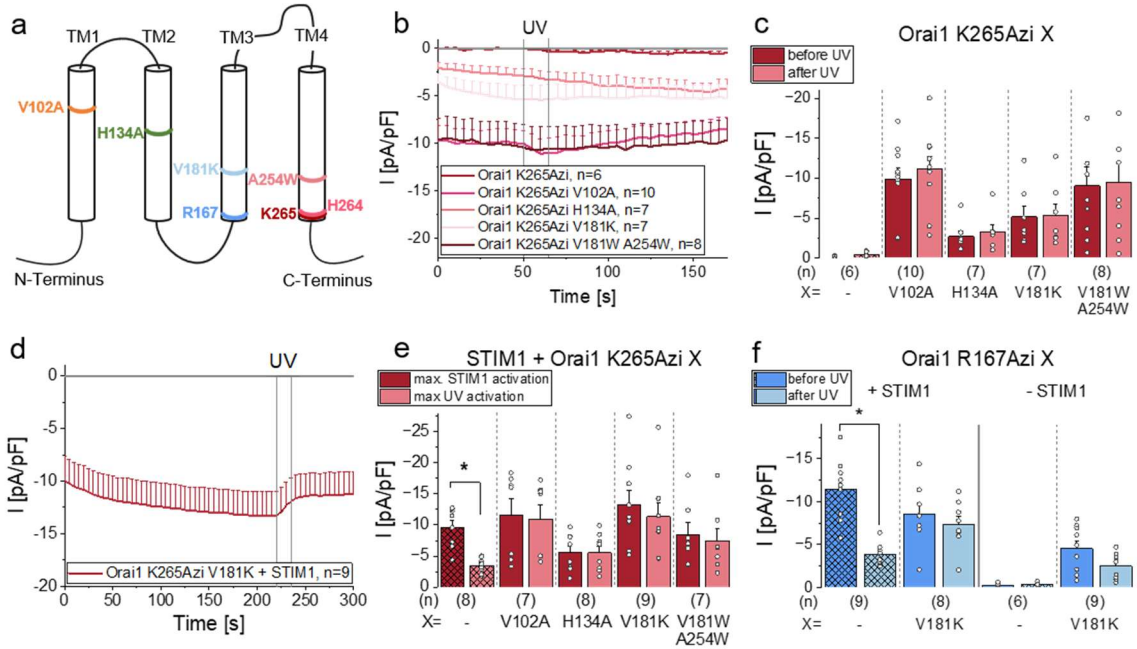

Figure 4: Combination of K265Azi/Bpa or R167Azi/Bpa with mutations triggering constitutive activity eliminates UV-induced current decrease

a) Schematic representation of the Orai1 subunit highlighting tested GoF-mutants in TM1-TM4. **b) d)** Time course of current densities after whole cell break-in of b) Orai1 K265Azi and Orai1 K265Azi V102A/H134A/V181K/V181W A254W in the absence of STIM1 and of d) Orai1 K265Azi V181K in the presence of STIM1. UV-light is applied for 15s at t= 50s (b)/ 220s (d). **c) e)** Bar diagrams exhibiting maximal current densities before and after 15s UV-illumination of Orai1 K265Azi and Orai1 K265Azi V102A/H134A/V181K/V181W A254W in the c) absence of STIM1 and e) presence of STIM1. Statistical significance before and after UV-illumination are indicated by asterisk * ($p < 0.05$). **f)** Bar diagram showing maximal current densities after STIM1-activation and after 15s UV-illumination of Orai1 R167Azi and Orai1 R167Azi V181K in the presence (left) and absence (right) of STIM1. Statistical significance before and after UV-illumination are indicated by asterisk * ($p < 0.05$). Single values are indicated as grey circles. Data represent mean values ± SEM of indicated number (n) of experiments. Detailed statistic values are shown in Supplementary Table 1.

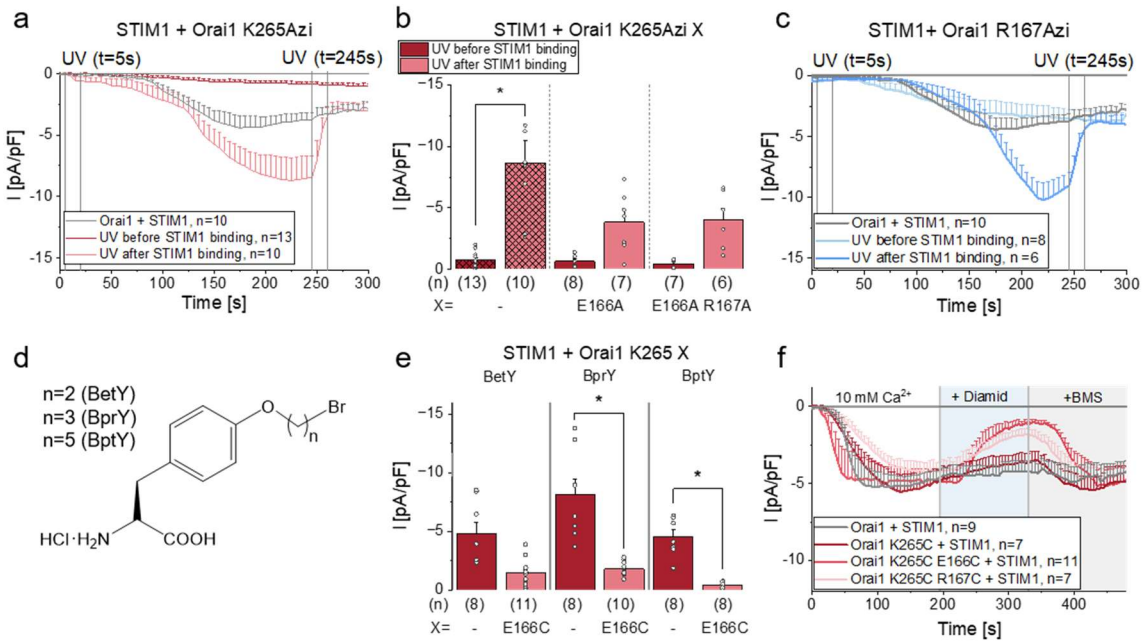

Figure 5: Restraining the nexus-TM3 interface via photo- and chemical crosslinking impairs STIM1-mediated maximal activation

a) c) Time course of current densities after whole cell break-in of Orai1 WT compared to a) Orai1 K265Azi and c) Orai1 R167Azi, with 15s UV-illumination before (at t= 5s) and after (at t= 245s) STIM1-binding. **b)** Bar diagram showing maximal STIM1-mediated current densities of Orai1 K265Azi and Orai1 K265Azi E166A/E166A R167A, with 15s UV-illumination before (at t= 5s) and after (at t= 245s) STIM1-binding. Statistical significance between both conditions of UV-illumination are indicated by asterisk * ($p < 0.05$). **d)** Chemical structure of chemical cross-linking UAAs with different linker length n. **e)** Bar diagram depicting maximal STIM1-mediated current densities of Orai1 K265-BetY/BprY/BptY and Orai1 K265-BetY/BprY/BptY E166C in the presence of STIM1. Statistical significance between single and double mutant containing a cysteine are indicated by asterisk * ($p < 0.05$). **f)** Time course of current densities after whole cell break-in of Orai1 WT, Orai1 K265C and Orai1 K265C E166C/ R167C in the presence of STIM1. The application of diamide is indicated by the blue background (at t= 195s) and of BMS by the grey background (at t= 330s). The respective application was performed after maximal or minimal currents were reached, respectively. Single values are indicated as grey circles. Data represent mean values ± SEM of indicated number (n) of experiments. Detailed statistic values are shown in Supplementary Table 1.

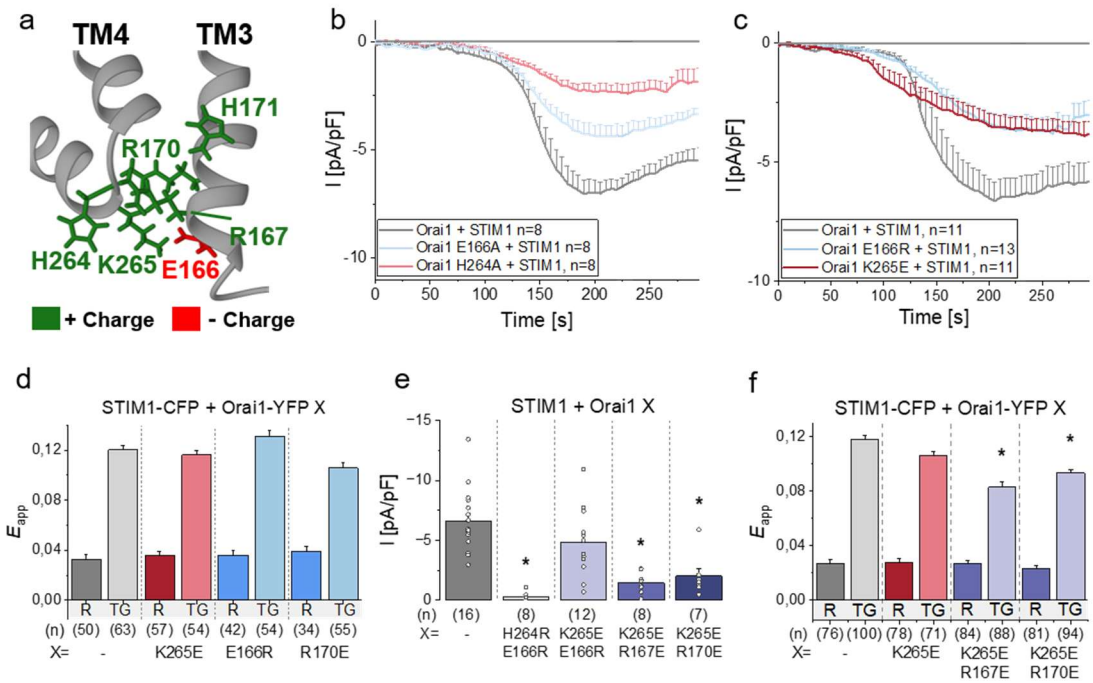

Figure 6: STIM1-coupling to and STIM1-mediated activation of Orai1 require charges in the nexus-TM3 interface

a) Representative scheme of positively (green) and negatively (red) charged residues in the Orai1 nexus-TM3 interface. **b) c)** Time course of current densities after whole cell break-in of Orai1 WT and b) Orai1 E166A/ H264A and c) Orai1 E166R/ K265E in the presence of STIM1. **d) f)** Bar diagrams depicting FRET efficiency (E_{app}) detecting the interaction of STIM1-CFP with Orai1-YFP WT and d) Orai1-YFP K265E/E166R/R170E and f) Orai1-YFP K265E/ K265E R167E/R170E at resting conditions (R) and after store-depletion with 1 µM Thapsigargin (TG). Statistical significance of Orai1 mutants compared to Orai1 WT at similar conditions are indicated by asterisk * ($p < 0.05$). **e)** Bar diagrams showing maximal current densities of Orai1 WT and Orai1 H264R E166R/K265E E166R/K265E R167E/K265E R170E in the presence of STIM1. Statistical significance of Orai1 mutants compared to Orai1 WT are indicated by asterisk * ($p < 0.05$). Single values are indicated as grey circles. Data represent mean values ± SEM of indicated number (n) of experiments. Detailed statistic values are shown in Supplementary Table 1.

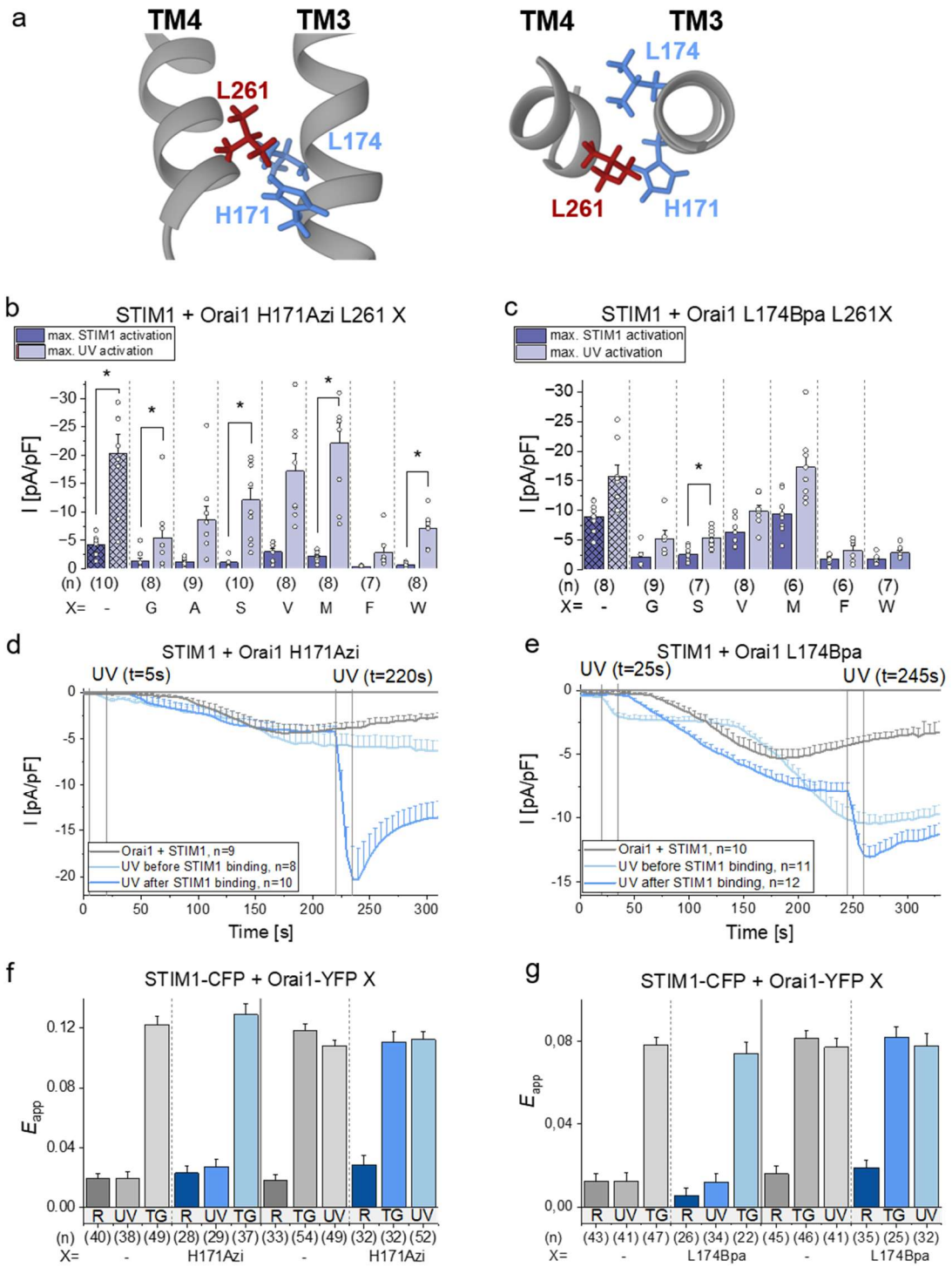

Figure 7: Photocrosslinking UAAs located on the opposite side of the upper hydrophobic nexus exhibit strong UV-mediated current activation

a) Schematic representation of the side view (left) and top view (right) of the upper nexus-TM3 interface highlighting key residues H171, L174 (TM3) and L261 (TM4). **b) c)** Bar diagrams showing maximal current densities after STIM1-activation and 15s UV-illumination of b) Orai1 H171Azi L261G/A/S/V/M/F/W and c) Orai1 L174Bpa L261G/S/V/M/F/W in the presence of

1003 STIM1. Statistical significance before and after UV-illumination are indicated by asterisk * ($p<$
1004 0.05). **d) e)** Time course of current densities after whole cell break-in of Orai1 WT and d) Orai1
1005 H171Azi and e) Orai1 L174Bpa with 15s UV-illumination before (at t= 5s (d)/ 25s (e)) and after
1006 (at t= 220s (d)/ 245s (e)) STIM1-binding. **f) g)** Bar diagram showing FRET efficiency (E_{app})
1007 detecting the binding interaction of STIM1-CFP with Orai1-YFP WT and f) Orai1-YFP H171Azi
1008 and g) Orai1-YFP L174Bpa at resting conditions (R) and with 60s UV-illumination (UV) before
1009 (left) and after (right) store-depletion with 1 µM Thapsigargin (TG) triggering STIM1-binding.
1010 Data represent mean values ± SEM of indicated number (n) of experiments. Detailed statistic
1011 values are shown in Supplementary Table 1.

1012

1013